NASA TECHNICAL NOTE

NASA TN D-4629

C. 1

NASA TN D-4629

NAVIGATION AND GUIDANCE SYSTEMS PERFORMANCE FOR THREE TYPICAL MANNED INTERPLANETARY MISSIONS

by Flora B. Lowes and Thomas B. Murtagh

Manned Spacecraft Center
Houston, Texas

NATIONAL AERONAUTICS AND SPACE ADMINISTRATION • WASHINGTON, D. C. • JULY 1968

NAVIGATION AND GUIDANCE SYSTEMS PERFORMANCE FOR THREE TYPICAL MANNED INTERPLANETARY MISSIONS

By Flora B. Lowes and Thomas B. Murtagh

Manned Spacecraft Center
Houston, Texas

NATIONAL AERONAUTICS AND SPACE ADMINISTRATION

For sale by the Clearinghouse for Federal Scientific and Technical Information
Springfield, Virginia 22151 – CFSTI price $3.00

ABSTRACT

The navigation and guidance systems performance for manned interplanetary flight is evaluated for three representative missions: a 1972 Venus flyby mission, a 1975 Mars flyby mission, and a 1977 Mars orbital mission. The navigation system has both Earth-based radar and onboard tracking capabilities for updating position and velocity estimates for a spacecraft and an unmanned probe. Fixed-time-of-arrival and variable-time-of-arrival guidance logic is used in the guidance system to compute velocity corrections and target dispersions. From the performance evaluation for the three missions considered, arrival accuracies and propellant requirements can be predicted for the spacecraft and probe in the three types of missions presented or in similar interplanetary missions.

CONTENTS

Section	Page
SUMMARY	1
INTRODUCTION	1
SYMBOLS	2
ANALYSIS	5
Assumptions	5
Orbit-Plane Coordinate System	6
Trajectory Characteristics	6
Navigation and Guidance Systems Equations	7
RESULTS AND DISCUSSION	8
1972 Venus Flyby Mission	10
1975 Mars Flyby Mission	17
1977 Mars Stopover Mission	23
CONCLUDING REMARKS	29
APPENDIX — SPACECRAFT/PROBE NAVIGATION-SYSTEM EQUATIONS	35
REFERENCES	39

TABLES

Table		Page
I	EXPECTED 1σ ROOT-MEAN-SQUARE ERROR VALUES	30
II	REFERENCE TRAJECTORY CHARACTERISTICS	31
III	CHARACTERISTICS OF PARKING ORBIT FOR 1977 MARS STOPOVER MISSION	32
IV	MIDCOURSE ΔV AND TARGET-PLANET DISPERSION SUMMARY	33
V	PROBE ΔV AND DISPERSION SUMMARY	34

FIGURES

Figure		Page
1	Projection of trajectories into the ecliptic plane	
	(a) 1972 Venus flyby mission	7
	(b) 1975 Mars flyby mission	7
	(c) 1977 Mars stopover mission	7
2	Sighting-body position-measurement errors used to determine navigation schedule for 1972 Venus flyby mission trajectory	9
3	Sighting-body position-measurement errors used to determine navigation schedule for 1975 Mars flyby mission trajectory	9
4	Sighting-body position-measurement errors used to determine navigation schedule for 1977 Mars stopover mission trajectory	
	(a) Earth to Mars trajectory	10
	(b) Mars to Earth trajectory	10
5	Root-mean-square position uncertainty at target-planet periapsis for 1972 Venus flyby mission	
	(a) Earth to Venus trajectory	12
	(b) Venus to Earth trajectory	12
6	Spacecraft guidance accuracy for 1972 Venus flyby mission	
	(a) Venus approach phase (outbound)	14
	(b) Earth approach phase (return)	14
7	Unmanned-probe entry parameters as a function of separation velocity (1972 Venus flyby mission)	
	(a) Entry altitude = 490 000 feet	15
	(b) Entry altitude = 580 000 feet	15
8	Unmanned-probe navigation data for 1972 Venus flyby mission	16
9	Unmanned-probe guidance data for 1972 Venus flyby mission	16
10	Root-mean-square position uncertainty at target-planet periapsis for 1975 Mars flyby mission	
	(a) Earth to Mars trajectory	18
	(b) Mars to Earth trajectory	18

Figure		Page
11	Spacecraft guidance accuracy for 1975 Mars flyby mission	
	(a) Mars approach phase (outbound)	19
	(b) Earth approach phase (return)	19
12	Unmanned-probe entry parameters as a function of separation velocity (1975 Mars flyby mission)	
	(a) Entry altitude = 315 000 ft	21
	(b) Entry altitude = 405 000 ft	21
13	Unmanned-probe navigation data for 1975 Mars flyby mission	21
14	Unmanned-probe guidance data for 1975 Mars flyby mission	
	(a) Expected onboard-radar errors	22
	(b) Twice the expected onboard-radar errors	22
15	Root-mean-square position uncertainty at target-planet periapsis for 1977 Mars stopover mission	
	(a) Earth to Mars trajectory	24
	(b) Mars to Earth trajectory	24
16	Spacecraft guidance accuracy for 1977 Mars stopover mission	
	(a) Mars approach phase (outbound)	25
	(b) Earth approach phase (return)	25
17	Orbital navigation accuracy for 1977 Mars stopover mission	26
18	Unmanned-probe entry parameters as a function of separation velocity (1977 Mars stopover mission)	
	(a) Entry altitude = 315 000 ft	27
	(b) Entry altitude = 405 000 ft	27
19	Unmanned-probe navigation data for 1977 Mars stopover mission	28
20	Unmanned-probe guidance data for 1977 Mars stopover mission	
	(a) Expected onboard-radar errors	28
	(b) Twice the expected onboard-radar errors	28

NAVIGATION AND GUIDANCE SYSTEMS PERFORMANCE FOR THREE TYPICAL MANNED INTERPLANETARY MISSIONS

By Flora B. Lowes and Thomas B. Murtagh
Manned Spacecraft Center

SUMMARY

An analysis of the navigation and guidance systems for manned interplanetary flight is presented. The performance results, with state-of-the-art techniques assumed, are given for three representative mission types: Venus flyby, Mars flyby, and Mars orbital. The study includes analyses of all phases of each respective mission, with the outbound phase of each mission encompassing a performance evaluation for both the manned spacecraft and an unmanned probe.

The configuration for the midcourse navigation system includes both Earth-based radar and onboard tracking capabilities for updating position and velocity estimates of the spacecraft and probe obtained using a Kalman filter. The guidance system utilizes fixed- and variable-time-of-arrival guidance logic to compute the velocity corrections and appropriate target dispersions.

From the performance evaluation of the navigation and guidance systems for the three missions considered, conclusions can be drawn about arrival accuracies and propellant requirements for the spacecraft and probe pertaining to either these specific missions or other interplanetary missions with similar characteristics. Excluding the propellant requirement for maneuvers in the orbital phase of a Mars stopover mission, the results of the study indicate that a total midcourse velocity requirement for each of the missions considered is of the order of 200 fps, with resulting spacecraft arrival accuracies of 4 n. mi. at Mars or Venus and 1 n. mi. at Earth for the outbound and return mission phases, respectively. Similarly, for the probe delivery, an accuracy somewhat less than 5 n. mi. can be obtained, with only one velocity correction of approximately 80 fps.

INTRODUCTION

When considering manned interplanetary missions, it is assumed that the targets of primary scientific interest would be Venus or Mars. Thus, in the performance evaluation of the navigation and guidance systems for interplanetary missions, the reference missions chosen were a 1972 Venus flyby mission, a 1975 Mars flyby mission, and a 1977 Mars stopover mission. These specific missions were arbitrarily chosen for the analysis, since trajectory profile data were readily available. The purpose of

this study is not to recommend any specific mission, but to illustrate comparable systems performance for different mission types and to show that the results obtained are applicable to any mission with similar characteristics.

The reference missions chosen for the navigation and guidance systems analyses vary with total trip times of 363 days (Venus flyby mission), 672 days (Mars flyby mission), and 980 days (Mars stopover mission). The Mars stopover mission includes a 300-day orbital stay time about Mars. The Earth injection velocity and the Earth return velocity for each of the considered missions fit within the uprating capability of certain Apollo-Saturn systems.

The unmanned-probe reference trajectory for each mission is computed, assuming that the probe would be separated from the manned spacecraft at the target-planet sphere of influence (SOI). The inclination of the probe trajectory was assumed equal to the inclination of the spacecraft trajectory. The probe lead and lag times with respect to spacecraft arrival at the target-planet periapsis and with respect to the probe entry altitude, speed, and flight-path angle are calculated as a function of the probe separation ΔV.

For the analysis, all navigation types and schedules are considered to be consistent for each mission so that directly obtainable accuracies and propellant requirements can be compared. Use of a combination of Earth-based radar tracking and onboard sextant measurements was assumed for spacecraft navigation; whereas, use of a radar system on board the spacecraft was assumed for tracking the unmanned probe during its delivery phase. For the Earth-based radar observations, the existence of a network of three deep-space stations (Goldstone, Johannesburg, and Woomera) was assumed, with each viewing station measuring range and range-rate simultaneously. These radar data are corrupted by a variety of errors, but this analysis considers only the white-noise errors.

The assumptions used in the study are presented first, followed by a discussion of the reference trajectories used in the analysis and by a brief description of the navigation and guidance systems equations. The results and discussion of the data for the navigation and guidance systems analysis are presented in three sections, according to the mission studied. Each section devoted to a mission contains navigation and guidance systems discussions for both the manned spacecraft and the unmanned probe.

The authors wish to acknowledge the assistance of Victor R. Bond in generating the mission analysis reference trajectories and state transition matrices included in this report. The assistance of Joseph R. Thibodeau in developing the parking-orbit characteristics used in the 1977 Mars stopover mission is also acknowledged.

SYMBOLS

$A(t)$ sensitivity vector which relates star-planet-horizon angle deviations to state-vector deviations

$B(t)$ sensitivity matrix which relates relative range and range-rate deviations to state-vector deviations

$E(t)$	uncertainty covariance matrix
$E_p(t)$	probe uncertainty covariance matrix
$E_s(t)$	spacecraft uncertainty covariance matrix
$H(t)$	sensitivity matrix defined by equation (10)
I	identity matrix of appropriate dimensions
$K(t)$	weighting matrix defined in equation (15)
$M(t)$	3×3 matrix defined in equation (15)
$P(t)$	augmented uncertainty covariance matrix defined by equation (7)
$R(t)$	covariance matrix of measurement errors defined by equation (16)
r_B	target-planet radius
$\bar{r}_p$	unmanned-probe position vector with respect to target planet
r_s	magnitude of spacecraft position vector
$\bar{r}_s$	spacecraft position vector with respect to target planet
T_{VP}	time to vacuum periapsis
t	time
t_0	arbitrary initial time
$\hat{u}_s$	unit vector to star
$\bar{V}_p$	unmanned-probe velocity vector with respect to target planet
$\bar{V}_s$	spacecraft velocity vector with respect to target planet
$\bar{V}_\rho$	unmanned-probe relative velocity vector with respect to spacecraft, $\bar{V}_\rho = \bar{V}_p - \bar{V}_s$

$X(t)$	dispersion covariance matrix
β	angle between a star and the target-planet horizon line of sight
$\Gamma(t, t_0)$	unmanned-probe 6×6 state transition matrix
γ_e	unmanned-probe entry flight-path angle
$\Delta E(t)$	change to uncertainty covariance matrix as the result of a navigation measurement of a guidance maneuver
ΔV	change in velocity
$\Delta X(t)$	change to dispersion covariance matrix as the result of a guidance maneuver
$\delta( )$	small deviation
$\Theta(t, t_0)$	augmented 12×12 state transition matrix defined by equation (5)
θ	one-half the target-planet disk subtended angle, $\sin \theta = r_B/r_s$
$\vec{\xi}(t)$	augmented state-vector deviation defined by equation (4)
ρ	magnitude of relative position vector, range
$\vec{\rho}$	unmanned-probe relative position vector with respect to spacecraft, $\vec{\rho} = \vec{r}_p - \vec{r}_s$
$\dot{\rho}$	spacecraft/probe relative range-rate, $\dot{\rho} = \frac{\vec{\rho}}{\rho} \cdot \vec{V}_\rho$
σ_β^2	variance of star-horizon observable
σ_ρ^2	onboard-radar range variance
$\sigma_{\dot{\rho}}^2$	onboard-radar range-rate variance
$\Phi(t, t_0)$	spacecraft 6×6 state transition matrix

Subscripts:

1, . . . , 4	guidance-correction indices
sep	separation

Superscripts:

+	after navigation measurement or guidance maneuver
-	before navigation measurement or guidance maneuver
-1	inverse
T	transpose

ANALYSIS

Assumptions

The following ground rules are postulated for the mission analysis.

1. The Earth injection covariance matrix was diagonal, with root-mean-square (rms) position and velocity errors of 4 n. mi. and 16 fps, respectively. These values are consistent with current Manned Space Flight Network (MSFN) tracking capabilities for vehicles in Earth orbit.

2. The reference trajectories were calculated using matched conic techniques, and the state transition matrices used to propagate the errors were derived analytically for two-body conic trajectories.

3. The midcourse navigation-system configuration includes both Earth-based radar and onboard tracking capability for updating the spacecraft position and velocity estimates obtained using a Kalman filter. Earth-based radar range and range-rate data were processed for the time when the spacecraft is within the Earth sphere of influence (ESOI), and use of onboard optical tracking was assumed for the remaining phases of the missions. The relatively unusual combination of Earth-based tracking and autonomous navigation was employed in order to produce conservative performance results.

4. The assumed Earth-based radar error model is discussed in reference 1. The error model for the onboard sextant is considered to be the sum of three error sources, which are assumed to be uncorrelated with respect to each other and are uncorrelated from one observation to the next. The first source of error is the basic instrument error, the second is in the knowledge of the radius of the observed body, and the third results from the uncertainty in the position of the observed body (ref. 2).

5. For the onboard measurements, the visibility constraint was imposed that the angle between the lines of sight to a star or planet and the line of sight to the Sun be greater than 15°. No maximum angle constraint was imposed on the sextant field of view.

6. Fixed-time-of-arrival (FTA) and variable-time-of-arrival (VTA) guidance laws were used to compute the rms velocity corrections and appropriate target dispersions for both the spacecraft and the unmanned probe. These guidance laws are discussed in references 2 and 3. The VTA guidance law was used inside the target-planet SOI, with the FTA guidance law used in other mission phases. The schedules for midcourse velocity corrections were nonoptimum, but were selected in such a manner that rms radius-of-periapsis dispersions of less than 5 n. mi. are produced during each planet approach phase, including during Earth return.

7. The midcourse ΔV execution error was assumed to be a function of random errors in engine cut-off and in thrust-vector orientation and magnitude. These guidance errors are directly related to accelerometer bias and scale factor errors, gyro drift and platform misalinement, and engine tail-off errors.

8. The unmanned-probe reference trajectory was computed, assuming that the probe would be deployed from the manned spacecraft at the target-planet SOI and that the inclination of the probe trajectory would be equal to that of the spacecraft trajectory. Use of an onboard-radar system capable of measuring relative range and range-rate was assumed for spacecraft/probe tracking. An augmented Kalman filter (discussed in the appendix) was used to process spacecraft/probe tracking data simultaneously during this mission phase. The expected navigation and guidance systems errors are listed in table I. The navigation system errors were assigned conservative values to offset the omission of other system model errors.

Orbit-Plane Coordinate System

The rms position and velocity errors, computed from the square root of the trace of either the dispersion or the uncertainty covariance matrices, are presented in an orbit-plane coordinate system which displays both in-plane and out-of-plane errors. The X-axis (radius) of this system is along the radius vector from the central body to the spacecraft or probe; the Z-axis (track) is along the orbital angular-momentum vector; and the Y-axis (range) completes the orthogonal right-handed triad. The designated errors in this system therefore occur in radius, range, and track and in their time rates of change.

Trajectory Characteristics

The missions considered for this study were a 1972 Venus flyby mission, a 1975 Mars flyby mission, and a 1977 Mars stopover mission. The reference trajectory characteristics for these missions are summarized in table II. The stopover mission orbital parameters are presented in table III. The projections of the three mission trajectories in the ecliptic plane are illustrated in figure 1.

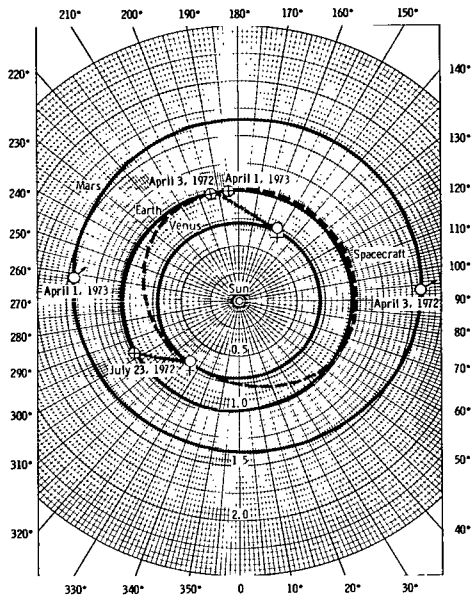

(a) 1972 Venus flyby mission.

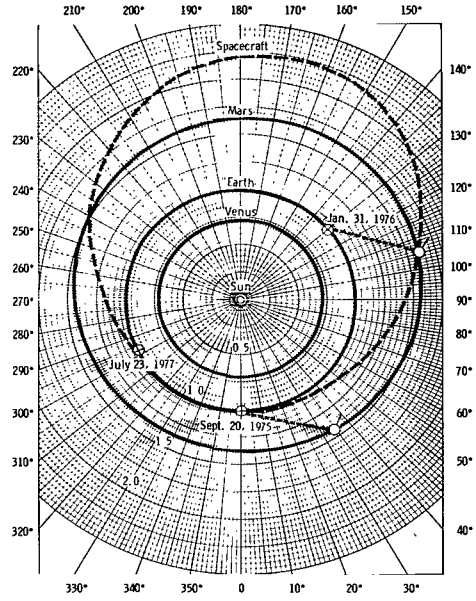

(b) 1975 Mars flyby mission.

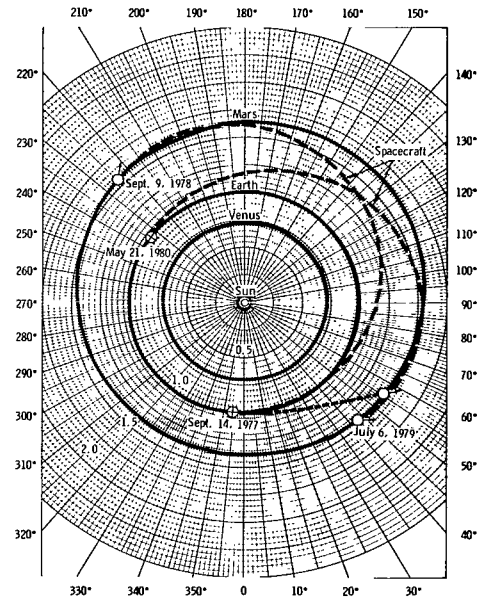

(c) 1977 Mars stopover mission.

Figure 1. - Projection of trajectories into the ecliptic plane.

Navigation and Guidance Systems Equations

The pertinent error matrices usually referred to in navigation and guidance systems analyses are the uncertainty covariance matrix E(t) and the dispersion covariance matrix X(t). The uncertainty matrix is a measure of the distance between the estimated trajectory and the trajectory actually being flown; the dispersion matrix represents the deviation of the actual trajectory from the nominal. The linearized error-analysis equations used to update E(t) and X(t) as the result of a navigation measurement or guidance maneuver are discussed extensively in references 1, 2, 3, and 4 and can be written in a generalized form as

$$E(t) = \Phi\left(t, t_0\right) E\left(t_0\right) \Phi^T\left(t, t_0\right) + \Delta E(t) \qquad (1)$$

and

$$X(t) = \Phi(t, t_0) X(t_0) \Phi^T(t, t_0) + \Delta X(t) \tag{2}$$

where $\Phi(t, t_0)$ is the state transition matrix which relates state-vector perturbations at time t to state-vector perturbations at time t_0.

If a navigation measurement is processed at time t, then $\Delta X(t) = 0$, and $\Delta E(t)$ is computed as a function of (1) the type of measurement, (2) the random errors associated with the data processed, and (3) the propagated uncertainty associated with the state-vector estimate at the time of a prior measurement or guidance maneuver.

When reasonable confidence is obtained in the trajectory estimate, guidance maneuvers are commanded in order to restore the dispersed trajectory to specified nominal conditions. If a guidance correction is executed at time t, $\Delta X(t)$ is computed as a function of (1) the guidance law implemented, (2) the errors associated with the imperfect thrusting maneuver, and (3) the dispersions propagated from the previous navigation measurement or guidance maneuver. The change to the uncertainty matrix $\Delta E(t)$ is calculated as a function of the thrust execution errors and propagated uncertainties from the previous navigation measurement or guidance maneuver.

If neither a navigation measurement nor a guidance maneuver is commanded, then $\Delta X(t) = \Delta E(t) = 0$, and the error matrices are propagated to the next decision point.

RESULTS AND DISCUSSION

Before navigation and guidance systems analyses can be performed and the results of the analyses compared for three different missions, navigation measurement types and schedules and guidance methods which are to be used must be determined. For this study, Earth-based tracking was assumed within the ESOI; whereas, outside the ESOI, navigation by an onboard system was assumed. By using onboard navigation outside the ESOI, errors in the ephemerides of the planets could be more easily included.

The following general discussion refers to the outbound and return phases of all three missions; discussion of the orbital phase of the 1977 Mars stopover mission is deferred to another section of this paper. Onboard navigation of the spacecraft was simulated, using a sextant to obtain included-angle measurements. During a heliocentric part of the outbound and return trajectories, star-planet included-angle measurements were processed at 0.5-day intervals. Within the target-planet SOI, measurement intervals were reduced to 30 minutes, and the type of measurement changed to that of star-horizon included-angle measurement. The two measurement types are discussed in references 2 and 4. The choice of time intervals for the measurement schedules was based on experience from previous studies.

No attempt was made to optimize the choice of stars for the sextant measurements. The star used for each measurement was randomly chosen from a limited catalog of stars in the simulation program. However, an attempt was made to establish some criteria for the selection of an optimum sighting body, other than the star, to be used for the optical measurements. The criteria were established by investigating the measurement accuracy obtained by the sextant for bodies of interest along the trajectory of each mission. As pointed out in reference 5, the position uncertainty established with an optical device is directly related to the range of the body being observed. Thus, for each observation, the uncertainty in the position measurement for each body of interest can be calculated. By this process, which is based on the range of the observed body and on optical-sighting variances, a semioptimum choice of a sighting body can be made.

The calculated errors in the position measurement are presented in figures 2 to 4 for each celestial body of interest during the 1972 Venus flyby, the 1975 Mars flyby, and the 1977 Mars stopover missions. From these figures, a reference navigation schedule of sighting bodies can be determined for each mission. Figures 2 to 4 are applicable only to the three missions in this study; however, a reference navigation schedule can be easily determined for any trajectory by using the same method on similar plots. In the following sections of this paper, figures 2 to 4 will be discussed in more detail for each mission.

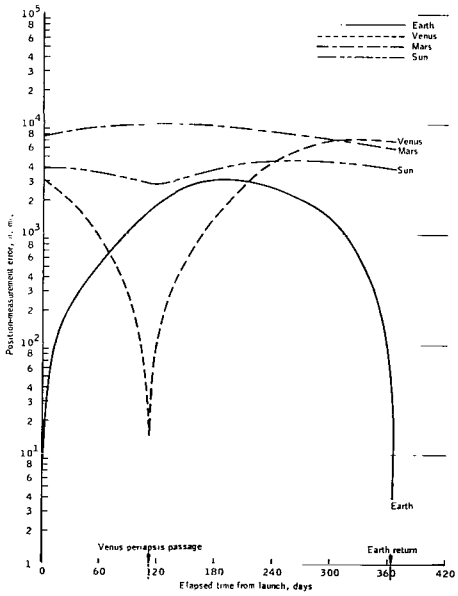

Figure 2. - Sighting-body position-measurement errors used to determine navigation schedule for 1972 Venus flyby mission trajectory.

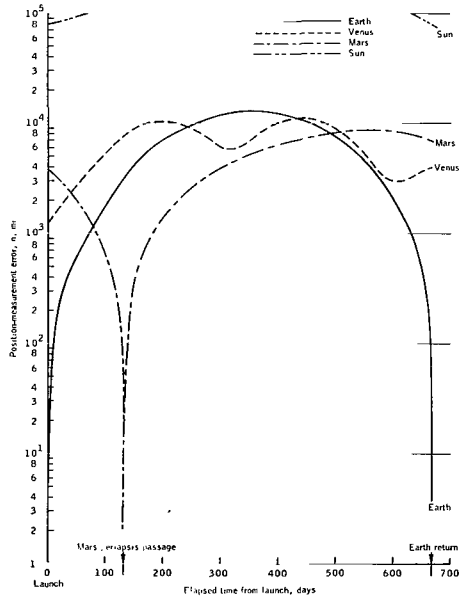

Figure 3. - Sighting-body position-measurement errors used to determine navigation schedule for 1975 Mars flyby mission trajectory.

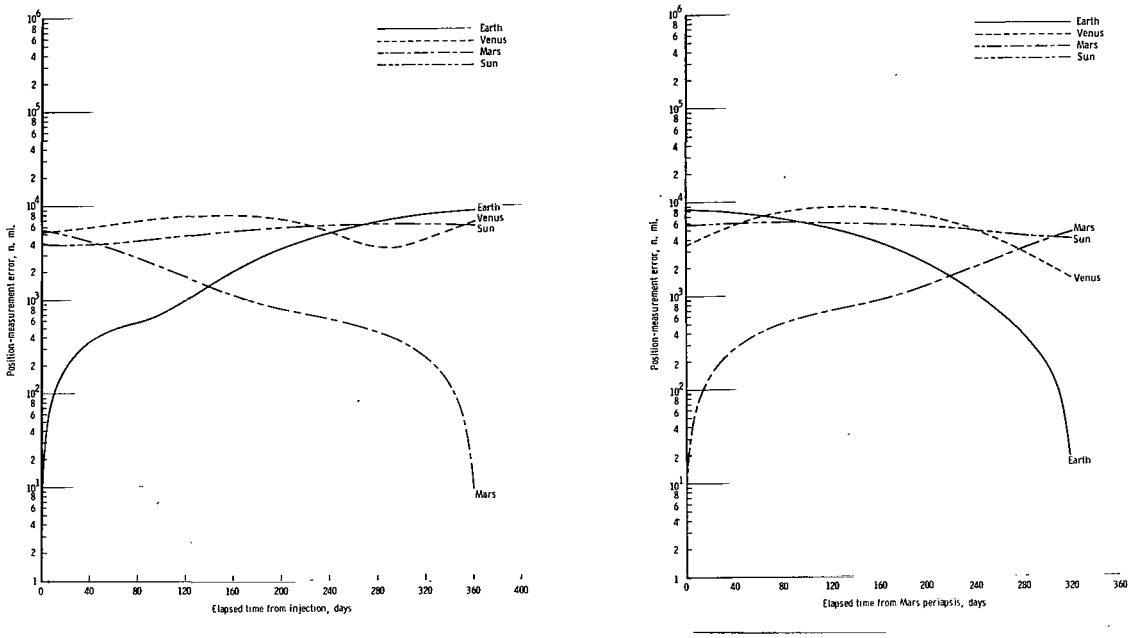

(a) Earth to Mars trajectory.

(b) Mars to Earth trajectory.

Figure 4. - Sighting-body position-measurement errors used to determine navigation schedule for 1977 Mars stopover mission trajectory.

After separation of the probe from the spacecraft during the outbound phase of each mission, navigation of the probe was accomplished by processing relative range and range-rate measurements obtained with radar on board the spacecraft. For this study, the probe entry parameters for each mission were chosen so that the required separation ΔV would be near the minimum value. However, in actual practice, these probe parameters would be chosen as a function of the specific type of mission technique considered (e.g., hard lander, soft lander, aerodynamic braking into orbit, etc.). The appendix contains the equation development pertinent to the probe delivery analysis. Spacecraft and probe midcourse performance results for all three missions are summarized in tables IV and V, respectively.

1972 Venus Flyby Mission

Spacecraft navigation and guidance. - A flyby mission is composed of two phases, the outbound phase and the return phase. The outbound phase is defined as that portion of the mission from injection at Earth to arrival at the target-planet periapsis, or in this case, at Venus periapsis. The return phase is similarly defined as the portion of the mission from the target-planet periapsis back to arrival at Earth. For the two phases of the Venus flyby mission, the navigation assumed is as previously described for all missions. From figure 2, a reference schedule pertaining to sighting-body selection for the star-planet measurements was determined. For example, for the

outbound phase of the mission, which has a time span of approximately 113 days (Venus periapsis passage), it is obvious that better measurement accuracy can be obtained by sighting on the Earth from injection until approximately 69 days into the mission, at which time Venus becomes the desired sighting body. In the return phase, Venus remains the best choice until late in the phase (approximately 210 days into the mission, or about 100 days after Venus periapsis passage), at which time the Earth again becomes the primary sighting body. As can be seen in figure 2, measurement errors would not be decreased by use of either the Sun or Mars as a sighting body.

Typical navigation accuracy data for a 1972 Venus flyby mission are contained in figure 5, which shows the spacecraft rms position uncertainty at Venus periapsis for the outbound phase of the mission and at Earth periapsis for the return phase of the mission. The results of the analysis are presented for the terminal points only, since only the position uncertainties at the terminal points of each mission phase are of interest.

Figure 5(a) contains the projected position uncertainty as a function of the outbound trajectory time. The accuracy degradation caused by the guidance system can be seen by the breaks in the curve which appear after each guidance maneuver denoted on the curve by arrows. The initially projected position uncertainty is large, as would be expected. However, the error is effectively reduced by the Earth-based tracking while the spacecraft is within the ESOI and remains static during the greater part of the heliocentric portion of the trajectory. As has been found from previous studies and from the analysis of data for the three missions considered, the spacecraft position uncertainty tends to decrease very slowly with measurements taken during the heliocentric portion of the trajectory. This characteristic seems to be independent of measurement frequency during this period. Conversely, when the spacecraft is within the target-planet SOI, the position uncertainty decreases rapidly and varies slightly, according to the measurement frequency. This fact is evident in figure 5(a), in which it can also be seen that even with appreciable guidance-system degradation during the latter portion of the outbound phase of the mission (when approaching Venus), the onboard navigation system rapidly decreases the uncertainty in spacecraft position estimation at Venus periapsis. The navigation data of total position error at the target planet, presented in the conventional manner, represent the combined errors in radius, range, and track. However, because only onboard navigation was used after ESOI passage, the major portion of the total rms position error lies in the down-range component, which affects only arrival time. Thus, performance (which is measured by radius error) is generally good even when the total error appears rather large (refs. 1 and 3).

Figure 5(b) contains position-uncertainty data for the return phase of the Venus flyby mission. These data are similar to those presented in figure 5(a) for the outbound phase. In figure 5(b), rms position uncertainty at Earth periapsis is presented as a function of time along the return trajectory as measured from Venus periapsis. The position-uncertainty curve profile for the return phase differs from that for the outbound phase of the Venus mission. This difference is partially the result of the longer time of the return phase and partially the result of the navigation configuration, which utilizes only onboard optical measurements from Venus periapsis passage to the ESOI. The onboard navigation system appreciably lowers the initially projected position uncertainty while within the Venus SOI. However, the error curve tends to level off at a higher value during the heliocentric period of the trajectory than during the

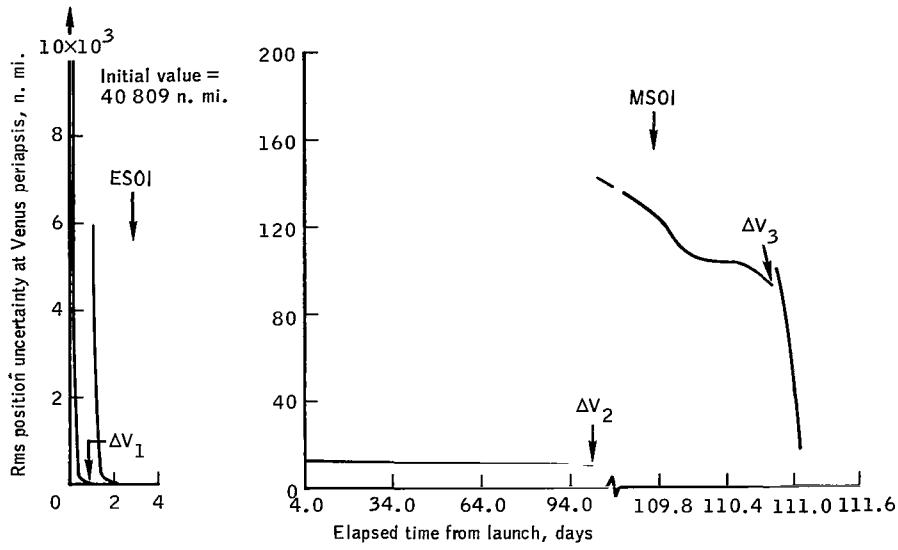

(a) Earth to Venus trajectory.

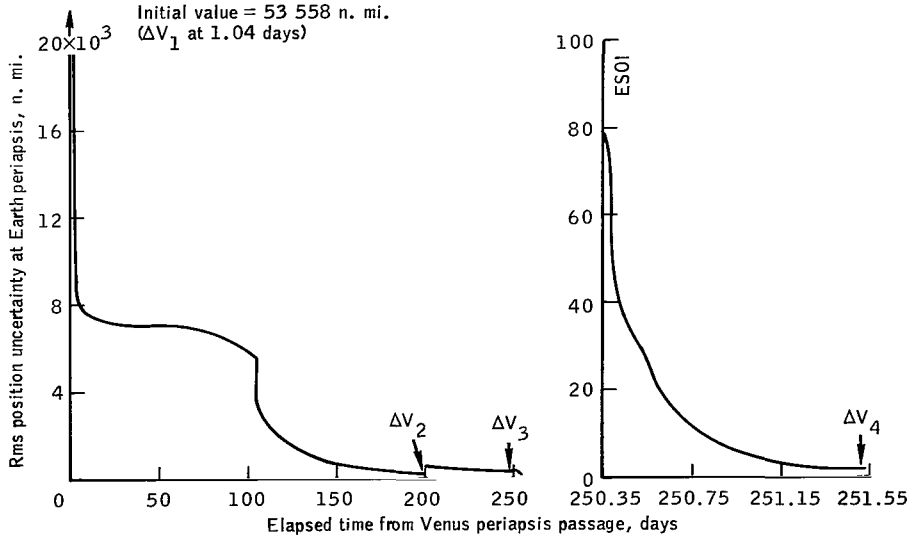

(b) Venus to Earth trajectory.

Figure 5. - Root-mean-square position uncertainty at target-planet periapsis for 1972 Venus flyby mission.

outbound phase. During the heliocentric period, little information is available for decreasing the errors in the state-vector estimate by using the navigation system. In figure 2, it is seen that during the early part of the return phase, the position-measurement error of the principal sighting body (i.e., Venus) increases until approximately 100 days, at which time the Earth comes within the range of the spacecraft, and information is contributed which will increasingly improve the navigation accuracy. In the position-uncertainty curve of figure 5(b), a marked decrease is noticed in the curve profile, and a continuous decrease occurs in the estimated position error during the remainder of the return phase. Once the spacecraft is within the ESOI, an appreciable increase in estimation accuracy is obtained by the use of Earth-based tracking. In figure 5(b), the rms position uncertainty for the spacecraft return to Earth is less than 2 n. mi., verifying the increase in estimation accuracy.

The decrease of the final position uncertainty obtained for the return phase, as contrasted to the position uncertainty for the outbound phase, can be attributed to the lack of any significant effect of guidance maneuvers on the navigation system. Since this particular mission is continuous, each correction is correlated with the execution errors of any previous corrections. In this study, the guidance-system degradation to navigation accuracy decreases with each correction. This decrease is evident from the curves in figure 5. The outbound phase clearly shows a significant decrease in position-estimation accuracy after each guidance maneuver. However, it is apparent that the effect of each maneuver tends to decrease until, in the return phase, the estimation-error curve is only slightly disturbed by a guidance maneuver.

As indicated in figure 5, seven guidance corrections were implemented for the 1972 Venus flyby mission. During the outbound phase, only three corrections were needed for the desired spacecraft delivery accuracy; whereas, four corrections were required for the desired accuracy in the return phase. Figure 6 contains the outbound and return midcourse ΔV as functions of spacecraft delivery accuracy at Venus and at Earth. The solid-line curves of figures 6(a) and 6(b) represent data obtained in the analysis using VTA guidance logic within the target-planet SOI; the dashed-line curves represent data obtained using FTA guidance logic. The dashed-line curves are provided for comparative purposes only. In an actual mission, the FTA guidance law would not be used during this particular time period since there is no need to control the down-range error and since, as shown in figure 6, the VTA guidance law produces better results for less ΔV. Thus, discussion will be limited to the curve for VTA guidance. Also, conclusions in this study will be based on the use of VTA guidance during the specific target-planet approach phases.

From figure 6(a), a total outbound ΔV budget can be determined as a result of the desired radius-of-periapsis dispersion. In this figure, the radius-of-periapsis dispersion at Venus is plotted against total rms outbound ΔV. The curve representing the VTA guidance can be used in choosing the final correction in the outbound phase. The last point on the curve at the right-hand side of figure 6(a) represents the second outbound correction at approximately 8 days from Venus periapsis passage. As can be seen, this second velocity correction resulted in a total ΔV of about 76 fps with a radius-of-periapsis dispersion of 32 n. mi. By following the profile of the dispersion curve, it can be readily determined whether or not any improvement can be made by a third guidance correction and, if so, when it should be made. Following the curve from right to left, it can be seen that in order to reduce the radius-of-periapsis dispersion to a tolerable value, it is necessary to wait until shortly before Venus periapsis

passage to execute the third velocity correction. In figure 6(a), an arrow denotes the choice of the third correction for this analysis. That is, for a ΔV of approximately 20 fps executed at 4 hours from periapsis, a delivery accuracy of 4 n. mi. can be realized at Venus periapsis passage, resulting in a total midcourse requirement of 96 fps for the outbound phase of the mission. The choice denoted is considered to be near optimum, since the dispersion gets no better and required ΔV increases rapidly beyond this point. This lower bound of delivery accuracy is dependent on the accuracy of the navigation system.

Figure 6(b) consists of information for the return phase of the 1972 Venus flyby mission. The data are plotted in the same manner as those in figure 6(a), and the total return ΔV and the placement of the fourth, or final, guidance correction for the return phase can be determined in a similar manner. In figure 6(b), the radius-of-periapsis dispersion at Earth is plotted as a function of the total rms return ΔV. Again, it is advantageous to wait until a few hours from periapsis to initiate the final velocity correction. From the curve representing VTA guidance, it is evident that the best delivery accuracy that can be obtained is approximately 1 n. mi. This accuracy costs, in turn, only 30 fps more than had been expended after the third correction; or it costs, in total, 116 fps for the return phase of the 1972 Venus flyby mission. In figure 6(b), the time choice for the fourth correction is again denoted by an arrow. The improvement of the dispersion at Earth upon return, as compared to the outbound leg, is the result of the improved navigation accuracy from longer onboard tracking during the heliocentric period and from Earth-based tracking within the ESOI.

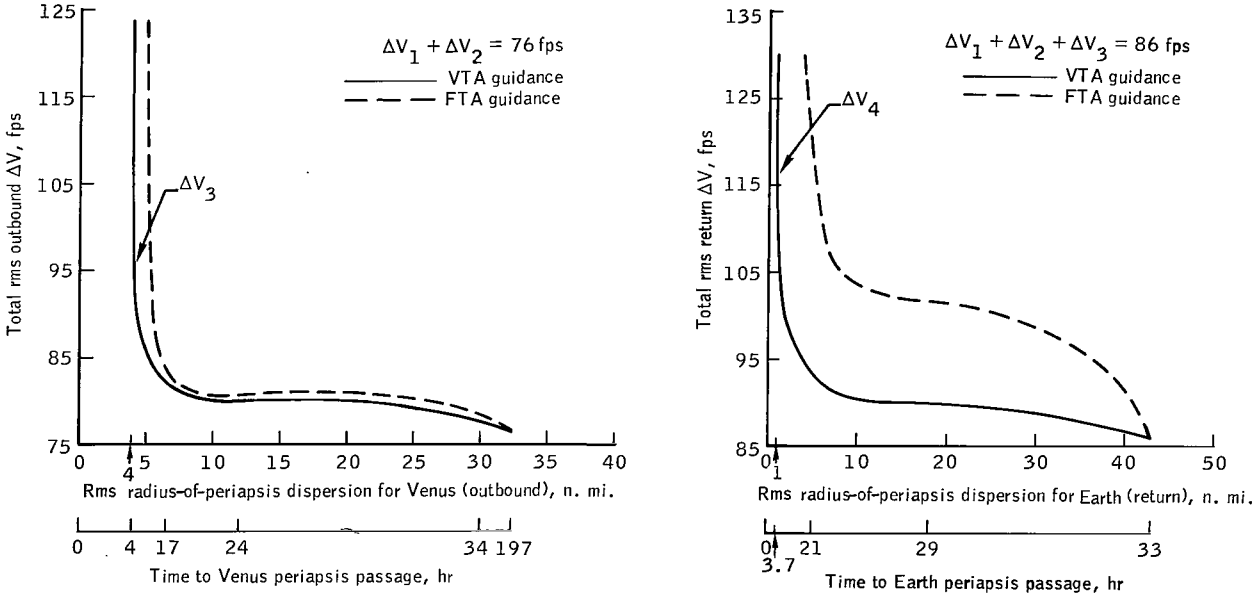

(a) Venus approach phase (outbound). (b) Earth approach phase (return).

Figure 6. - Spacecraft guidance accuracy for 1972 Venus flyby mission.

The figures previously discussed for the 1972 Venus flyby mission indicate that spacecraft delivery accuracies of 4 and 1 n. mi. can be obtained at Venus periapsis passage in the outbound phase and at Earth periapsis in the return phase, respectively. The cost of obtaining these delivery accuracies is approximately 96 fps for outbound and 116 fps for return, resulting in a total of 212 fps required for midcourse velocity maneuvers during the 1972 Venus flyby mission.

Unmanned-probe navigation and guidance. - Pertinent probe entry parameters for the 1972 Venus flyby mission are plotted in figure 7 as functions of separation velocities. For these data, it is assumed that the probe would be deployed from the spacecraft at the Venus SOI (approximately 330 000 n. mi. from Venus) and that the inclination of the probe trajectory would be the same as the inclination of the spacecraft flyby hyperbola. The minimum separation velocity occurs when the angle between $\Delta\vec{V}_{sep}$ and the spacecraft velocity vector is 90°. In figure 7(a), probe entry data are presented, with an assumed entry altitude of 490 000 feet; in figure 7(b), the entry altitude assumed is 580 000 feet. The increase in the entry altitude has the effect of shifting all curves to the left so that the minimum separation velocity occurs for a smaller entry speed. Variations in the entry flight-path angle from 0° to -45°, for fixed entry speed and altitude, produce an increase in the required separation velocity and a decrease in the time at which the probe arrives at the planned vacuum periapsis.

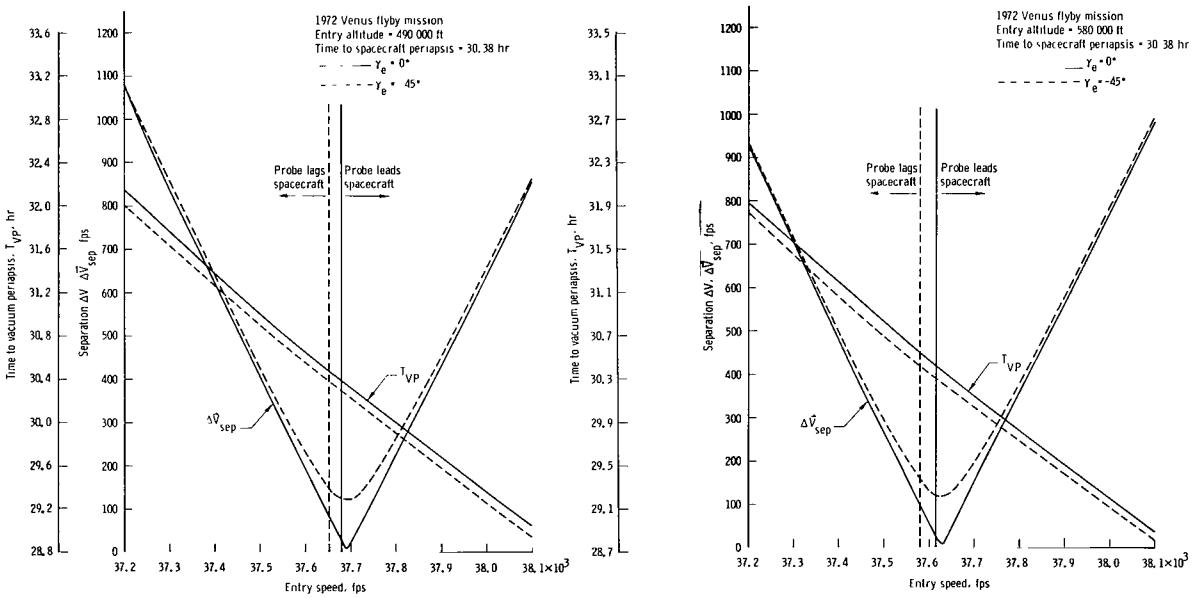

(a) Entry altitude = 490 000 feet. (b) Entry altitude = 580 000 feet.

Figure 7. - Unmanned-probe entry parameters as a function of separation velocity (1972 Venus flyby mission).

The choice of the probe entry trajectory has a definite effect on the delivery accuracy, but a parametric study to determine this influence is not included in this

report. For the analysis presented, the probe entry parameters were chosen so that a near-minimum separation velocity would be required. The entry altitude, speed, and flight-path angle specified were 490 000 feet, 37 670 fps, and -10°, respectively, with a corresponding separation velocity equal to 50 fps. With this choice of entry parameters, the probe arrives at its vacuum periapsis approximately 3 minutes after the spacecraft reaches the periapsis of the flyby hyperbola.

The probe navigation results for the 1972 Venus flyby mission are presented in figure 8. The significance of plotting the vacuum radius-of-periapsis error is better understood if it is realized that this single parameter is a measure of the entry corridor attainable by the probe midcourse navigation or guidance system. (The entry corridor = vacuum radius-of-periapsis error multiplied by 6.) The uncertainty and dispersion in this parameter are performance indices for the probe navigation and guidance systems, respectively. The uncertainty in vacuum radius of periapsis, illustrated in figure 8, is relatively insensitive to onboard-radar accuracy. The difference in the uncertainties for the expected radar errors (σ_ρ = 50 feet, $\sigma_{\dot\rho}$ = 0.5 fps) and that for twice the expected values is most pronounced around 14 hours from separation. The two curves converge, however, after 28 hours of tracking (56 measurements).

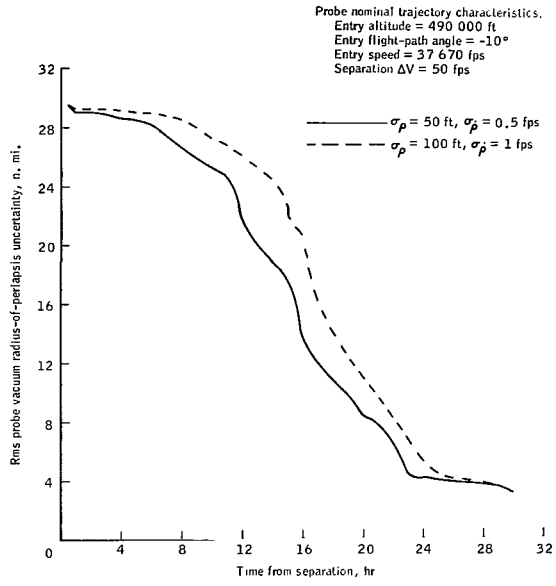

Figure 8. - Unmanned-probe navigation data for 1972 Venus flyby mission.

The probe midcourse guidance results are illustrated in figure 9. Only the data for the expected radar tracking errors are presented, since the midcourse ΔV profile for twice the expected radar errors is essentially the same. A single correction executed 1.5 hours before the probe arrives at its vacuum periapsis requires a ΔV equal to 35 fps, with a resulting corridor of 22.2 n. mi. (The vacuum radius-of-periapsis dispersion = 3.7 n. mi.) If this correction is delayed 1 hour, the corridor attainable using the midcourse guidance system can be reduced to 19.8 n. mi. for an increased ΔV of 108 fps.

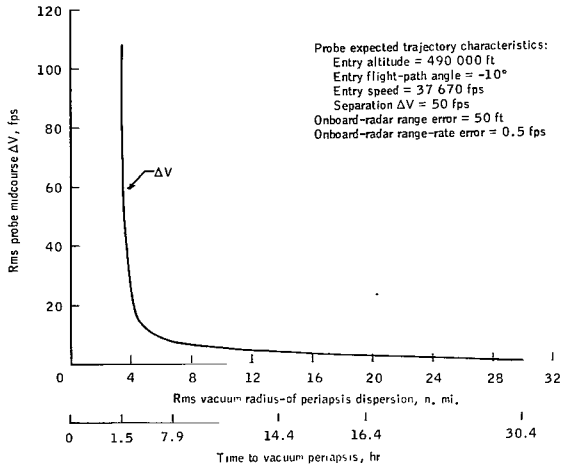

Figure 9. - Unmanned-probe guidance data for 1972 Venus flyby mission.

1975 Mars Flyby Mission

Spacecraft navigation and guidance. - The 1975 Mars flyby mission is similar to the 1972 Venus flyby mission in that it is a flyby mission with no stopover time at the target planet. This mission consists of an outbound phase of 133 days and a return phase of 539 days, resulting in a total round-trip time of 672 days. The navigation and guidance systems assumed for the 1975 Mars flyby mission are equivalent to those previously discussed for all three missions. Similarly, the optimum sighting-body schedule for the star-planet measurements was chosen from inspection of a plot of sextant-obtained measurement accuracies for bodies of interest along the trajectory. Figure 3 was used to determine the reference schedule for the 1975 Mars flyby mission. In figure 3, it is seen that Earth is to be used as the sighting body for the first 80 days of the outbound phase. At this time, Mars becomes the prominent sighting body and is used until almost 500 days into the mission, or about 360 days after Mars periapsis passage. From this point, Earth again is the obvious choice. As can be seen in figure 3, Earth and Mars do not always contribute significant navigation information; however, the other bodies along the trajectory cannot contribute as much as Mars or Earth. The effects of the fluctuations in the measurement-error curves of figure 3 can be seen in the navigation accuracy curves in figure 10.

Figure 10 contains the spacecraft rms position uncertainty at Mars periapsis for the outbound phase of the 1975 Mars flyby mission and at Earth periapsis for the return phase of the mission. As in the 1975 Venus flyby mission, the results here are also presented only for the terminal points of each phase.

In figure 10(a), the navigation accuracy obtained for the outbound phase of the Mars flyby mission is similar to that shown for the Venus flyby mission. The initially projected error is very large, but is effectively reduced early in the mission. The effects of the guidance-system degradation after each of the guidance maneuvers, which are denoted by arrows, can also be seen. Unlike the Venus outbound phase, which required three velocity corrections, the Mars outbound phase requires four velocity corrections to obtain the specified corridor at Mars periapsis. In figure 10(a), the final rms position uncertainty is approximately 40 n. mi. This uncertainty is twice the value obtained for the 1972 Venus flyby mission and is partially a result of the spacecraft decreased trajectory time within the Mars sphere of influence (MSOI). However, the largest portion of the position error is in the down-range component, which results in an arrival timing error; thus, position error does not affect the performance of the spacecraft.

Navigation data for the return phase of the 1975 Mars flyby mission are presented in figure 10(b), plotted in the same manner as the data for the outbound phase. Although the return phase is several hundred days longer than the outbound phase, four velocity corrections are sufficient. The uncertainty curve profile for the return phase of the 1975 Mars flyby mission behaves in much the same manner as that for the return phase of the 1972 Venus flyby mission. Again the guidance-system degradation is much less during the return phase, and the total rms position uncertainty is reduced to approximately 1 n. mi. at Earth periapsis.

Four velocity corrections are necessary during each phase of the 1975 Mars flyby mission; therefore, eight guidance maneuvers are required in order to obtain the

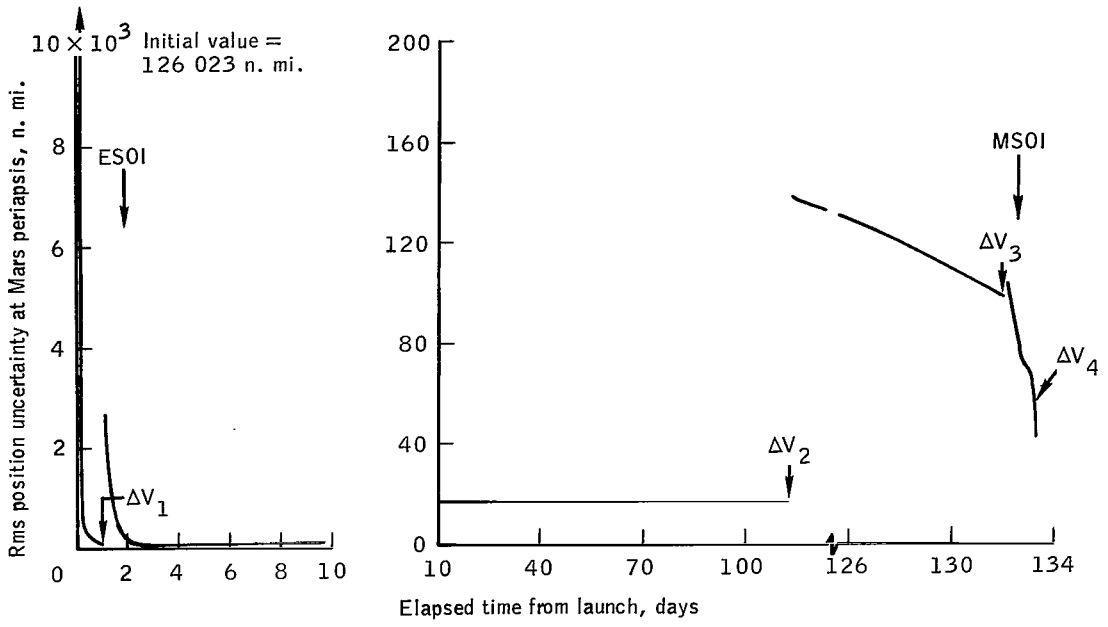

(a) Earth to Mars trajectory.

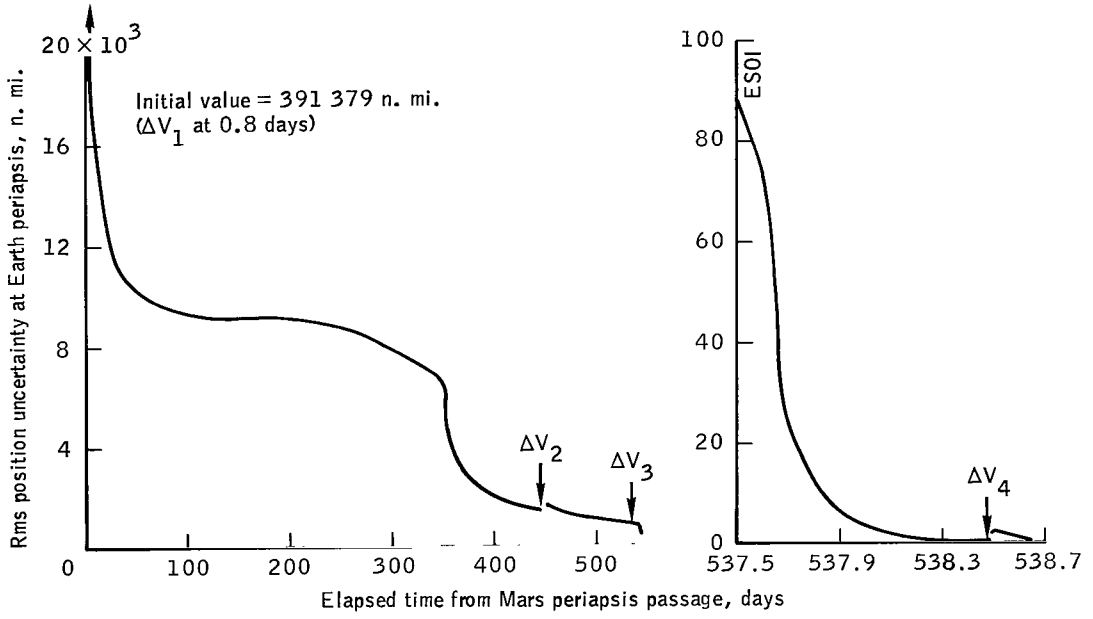

(b) Mars to Earth trajectory.

Figure 10. - Root-mean-square position uncertainty at target-planet periapsis for 1975 Mars flyby mission.

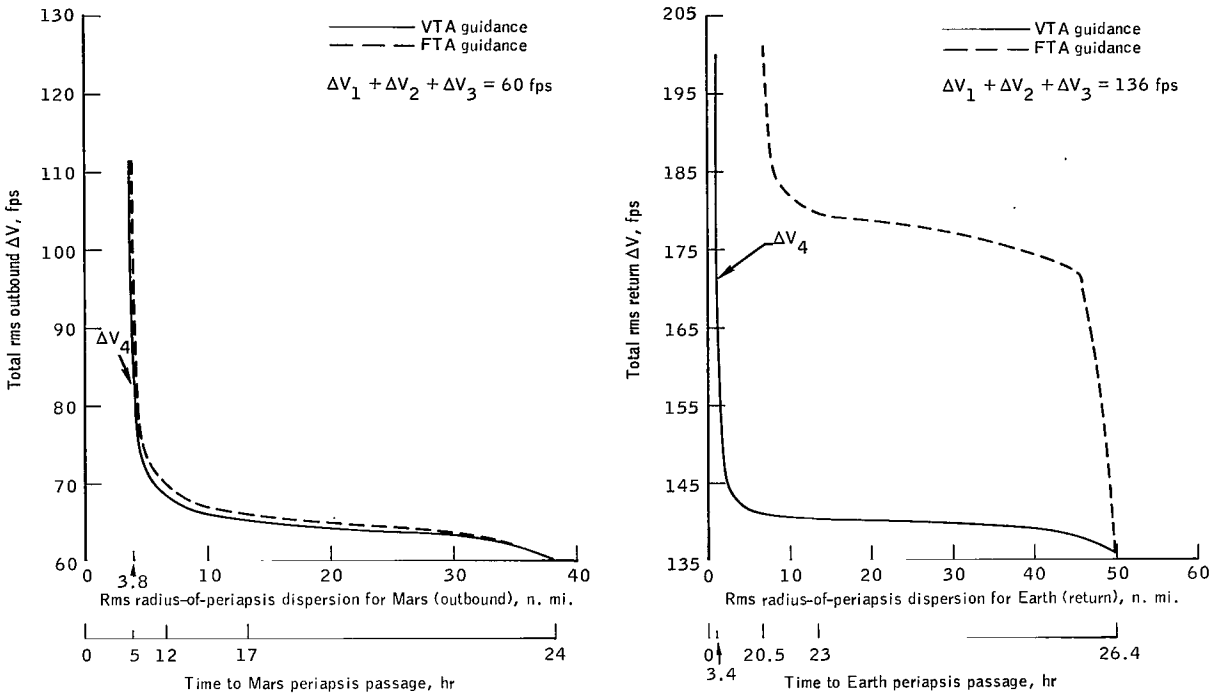

(a) Mars approach phase (outbound). (b) Earth approach phase (return).

Figure 11. - Spacecraft guidance accuracy for 1975 Mars flyby mission.

desired spacecraft delivery accuracy at Mars and Earth. Figures 11(a) and 11(b) contain the outbound and return midcourse ΔV plotted as functions of spacecraft delivery accuracy at Mars and at Earth, respectively. As was presented for the Venus mission, each plot contains a solid-line curve and a dashed-line curve representing data obtained with VTA guidance and with FTA guidance, respectively. For the 1975 Mars flyby mission, only the VTA guidance data will be discussed.

From figure 11, a total outbound and return ΔV budget can be determined, with reference to the desired radius-of-periapsis dispersion at the respective targets. In figure 11(a), the radius-of-periapsis dispersion at Mars is plotted against total rms outbound ΔV. Since the data begin after the third outbound velocity correction, the VTA guidance data curve can be used in choosing the final correction of the outbound phase. After the third correction, represented by the last point on the right-hand side of the plot, the total outbound rms ΔV equals 60 fps, and a delivery accuracy of approximately 37 n. mi. can be obtained. However, since the third correction is executed 24 hours before Mars periapsis passage and since the value of total ΔV required thus far is still rather low, a fourth velocity correction can be executed and a safe delivery accuracy obtained. Thus, using the same criteria as were used in the Venus mission, possibly the best choice for the fourth guidance maneuver is at 5 hours from periapsis passage. From figure 11(a), it can be seen that for approximately 12.5 fps more, or a total outbound rms ΔV of 82.5 fps, a radius-of-periapsis dispersion of less than 4 n. mi. can be obtained.

Similarly, from figure 11(b), the final velocity correction in the return phase of the 1975 Mars flyby mission can be chosen. The total return ΔV is, of course, dependent on the choice of corrections made and on the accuracy obtained during the outbound phase, since the flyby mission is a continuous mission.

Figure 11(b) consists of information for the return phase of the 1975 Mars flyby mission, plotted in the same manner as that in figure 11(a) for the outbound phase. In figure 11(b), the radius-of-periapsis dispersion at Earth is plotted against total rms return ΔV. Three velocity corrections are executed during the return phase at a cost of 136 fps for a delivery accuracy of 50 n. mi., and the final correction time can be chosen from the VTA guidance data curve in figure 11(b). As can be seen, the best obtainable accuracy is approximately 1 n. mi. For this delivery accuracy, a fourth correction must be made almost 3.5 hours from Earth periapsis at a cost of 35 fps, resulting in a total rms return ΔV of 171 fps. Again, as in the 1972 Venus flyby mission, the delivery accuracy is dependent on the navigation-system accuracy; thus, the use of Earth-based tracking during the return approach to Earth significantly aids in the improvement of the delivery accuracy, as compared to the accuracy achieved during the outbound approach to Mars.

The figures presented for the 1975 Mars flyby mission indicate that a manned spacecraft can be delivered to specified targets at Mars and Earth within accuracies of 4 and 1 n. mi., respectively. For this mission, the velocity corrections corresponding to these accuracies are approximately 83 fps for the outbound phase and 171 fps for the return phase, resulting in a total of 254 fps required for midcourse velocity maneuvers.

Unmanned-probe navigation and guidance. - Pertinent probe entry parameters for the 1975 Mars flyby mission are plotted in figure 12 as functions of separation velocity. The probe deployment from the spacecraft is assumed to occur at the MSOI (approximately 312 000 n. mi. from Mars), with the probe trajectory inclination the same as the inclination of the spacecraft flyby hyperbola. In figure 12(a), the probe entry data are presented for an entry altitude of 315 000 feet; in figure 12(b), the entry altitude assumed is 405 000 feet.

The probe reference trajectory characteristics for the navigation and guidance systems analysis are for an entry altitude, speed, and flight-path angle of 315 000 feet, 32 250 fps, and -10°, respectively, with a separation ΔV of 14 fps. With this choice of entry parameters, the probe arrives at vacuum periapsis 2 minutes before the spacecraft reaches the periapsis of the flyby hyperbola.

The probe navigation results for the expected and twice the expected onboard-radar errors are presented in figure 13. The radar errors representing twice the expected values degrade the projected estimate of the vacuum radius of periapsis during most of the tracking period, and the two curves eventually converge to the same value 18 hours after separation (36 measurements).

The midcourse guidance results for this mission are presented in figure 14. Figure 14(a) contains the guidance data for the expected radar errors, while figure 14(b) illustrates the guidance data for twice the expected onboard-radar errors. A single correction executed 48 minutes before the probe reaches vacuum periapsis produces a target dispersion of 4.1 n. mi. for a ΔV of 81 fps (σ_ρ = 50 feet, $\sigma_{\dot{\rho}}$ = 0.5 fps);

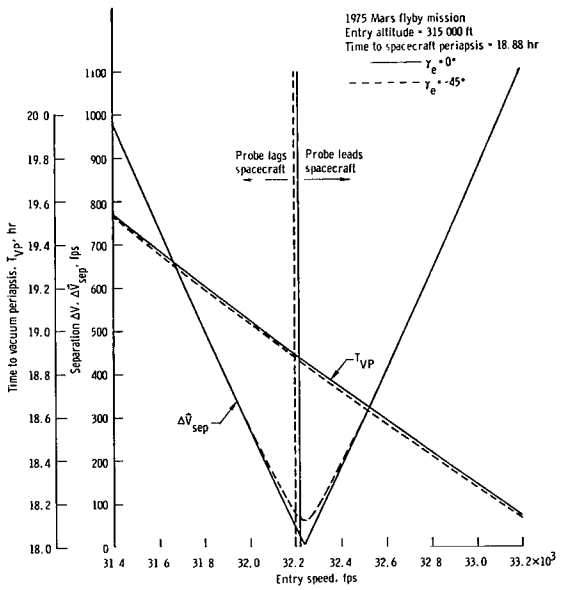

(a) Entry altitude = 315 000 ft.

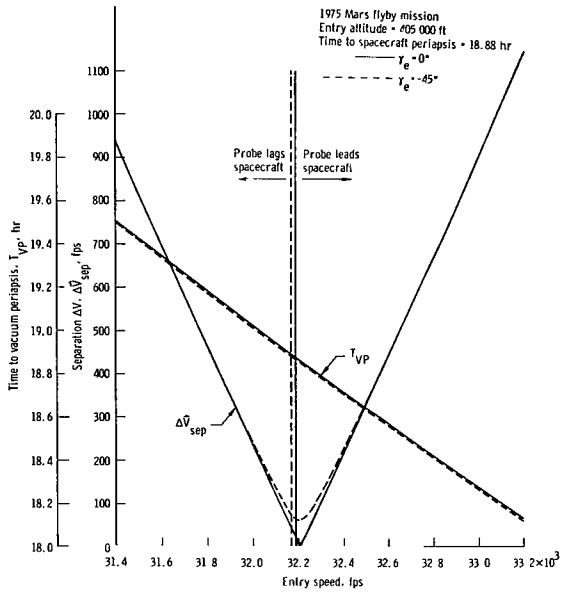

(b) Entry altitude = 405 000 ft.

Figure 12. - Unmanned-probe entry parameters as a function of separation velocity (1975 Mars flyby mission).

increasing the radar errors by a factor of 2 and computing the effect of a single correction at the same time and for the same ΔV produce a radius-of-periapsis dispersion of 6.8 n. mi. at vacuum periapsis. This disparity indicates that, for this mission, an increase in radar tracking errors has a pronounced effect on the guidance corridor. For example, if the specified guidance corridor is 30 n. mi., then the increase in tracking errors results in the probe not achieving the specified conditions. This corridor requirement can be satisfied, however, in the case of the increased tracking errors if the correction is delayed for 30 minutes. Then the corridor can be reduced to 19.8 n. mi. (radius-of-periapsis dispersion = 3.3 n. mi.) with an increased ΔV penalty of 195 fps.

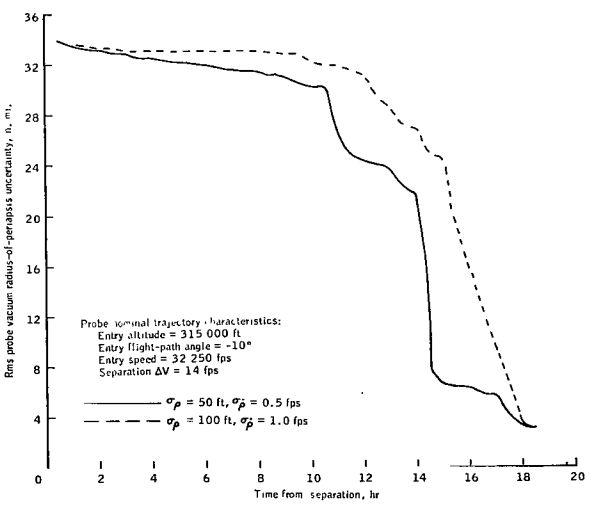

Figure 13. - Unmanned-probe navigation data for 1975 Mars flyby mission.

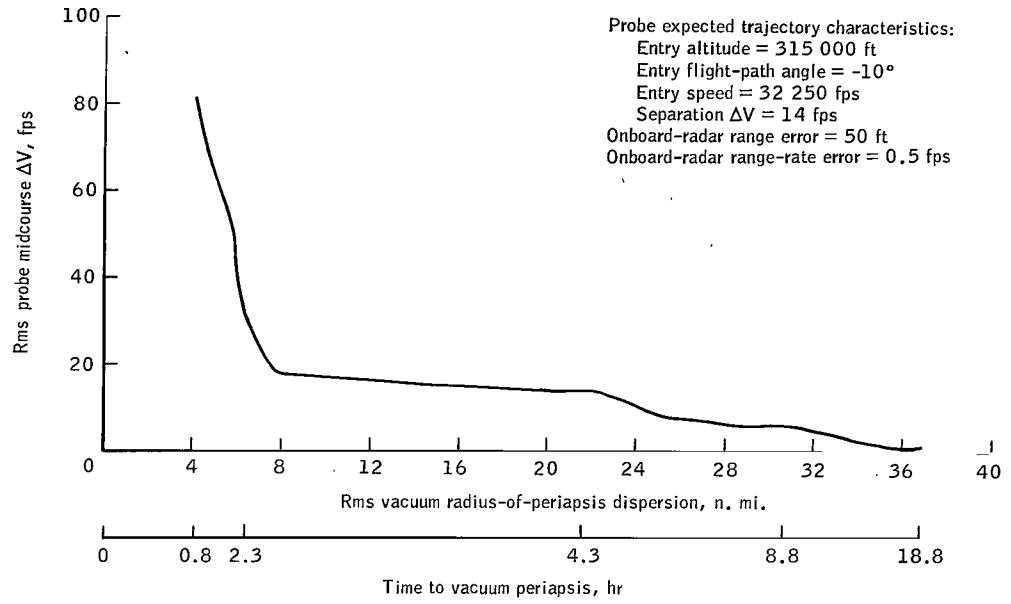

(a) Expected onboard-radar errors.

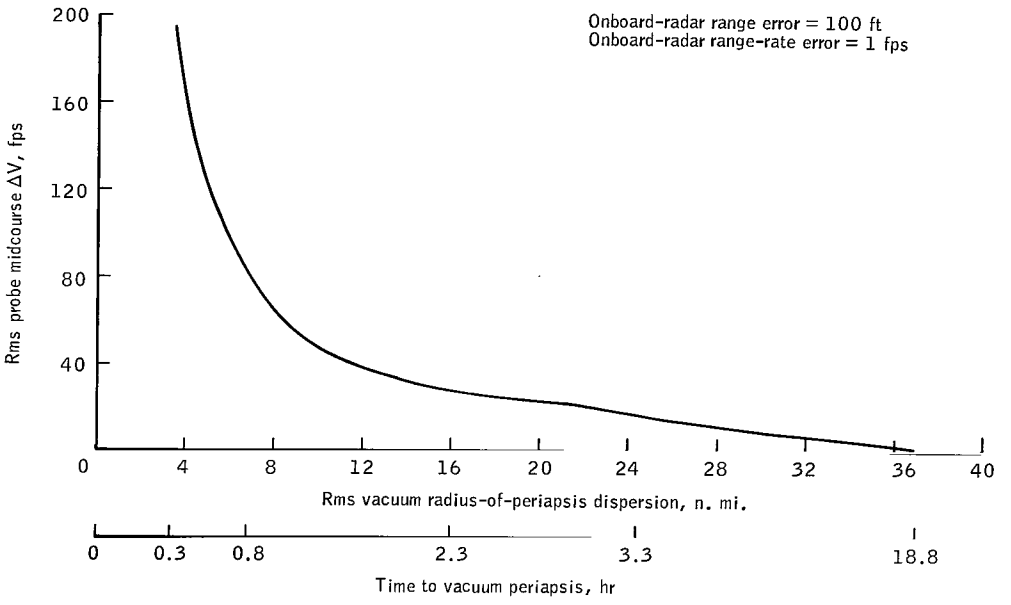

(b) Twice the expected onboard-radar errors.

Figure 14. - Unmanned-probe guidance data for 1975 Mars flyby mission.

1977 Mars Stopover Mission

Spacecraft navigation and guidance, outbound and return phases. - As opposed to the two flyby missions previously presented, the third mission of the analysis is a Mars stopover orbital mission. This mission consists of a 360-day outbound phase, a 300-day parking-orbital phase, and a 320-day return phase. The orbital phase is discussed separately, and the outbound and return phases are discussed simultaneously in order to make a comparison conveniently.

The navigation and guidance systems configuration assumed for the outbound and return phases of the 1977 Mars stopover mission is equivalent to that previously discussed for the flyby missions. Using the position-measurement error plotted in figure 4, reference schedules, pertaining to the optimum sighting body for the star-planet measurements, are chosen for the outbound and return phases. Figure 4(a) contains the position-measurement error as a function of time from injection at Earth. From this figure, it is evident that the Earth is the optimum sighting body for the onboard optical measurements during the first 140 days of the outbound trip phase. From this time until Mars periapsis, Mars is the optimum sighting body. Similarly, in figure 4(b), it is evident that Mars is the optimum sighting-body choice for the first 220 days of the return phase and that Earth is the optimum sighting-body choice for the remaining trip time.

Navigation uncertainty data for the 1977 Mars stopover outbound and return phases can be found in figure 15. From this figure, a close similarity to the previous figures is found, and the same types of data are plotted for the Mars stopover mission as were plotted for the Venus and Mars flyby missions. The principal difference can be seen in the slightly higher initial and intermediate uncertainty values for both the outbound and the return phases. This difference is the result of the much longer time period of both phases of the 1977 Mars stopover mission as compared to the time periods for each of the previous missions discussed. Also, it should be remembered that there is a time period of 300 days between the end of the outbound phase and the beginning of the return phase.

Figure 15 contains the rms position uncertainties at Mars periapsis and at Earth periapsis as functions of time along the outbound and return trajectories, respectively. In order to meet the specified delivery accuracy requirements, four guidance maneuvers are required in each phase, and these velocity corrections are denoted in figure 15 by arrows. In this figure, the terminal position uncertainty for each phase is approximately equal to the terminal position uncertainty for each respective phase of the two flyby missions. In figure 15(b), the curve profile levels off during the long heliocentric period of the return phase, when very little navigation information is obtained; and the curve drops appreciably at approximately 220 days, when the Earth again becomes the optimum sighting body.

Figure 16 contains the total outbound and return rms ΔV as a function of rms radius-of-periapsis dispersion at Mars and at Earth, respectively. This figure was used to determine the fourth correction of each phase of the 1977 Mars stopover mission, in the same manner as the fourth correction was determined for the Venus and Mars flyby missions. That is, in figure 16(a), after the third velocity correction of the outbound phase, the delivery accuracy of the spacecraft to Mars periapsis (or orbital insertion) is 26 n. mi., and the total cost at this time is 74 fps. From the VTA

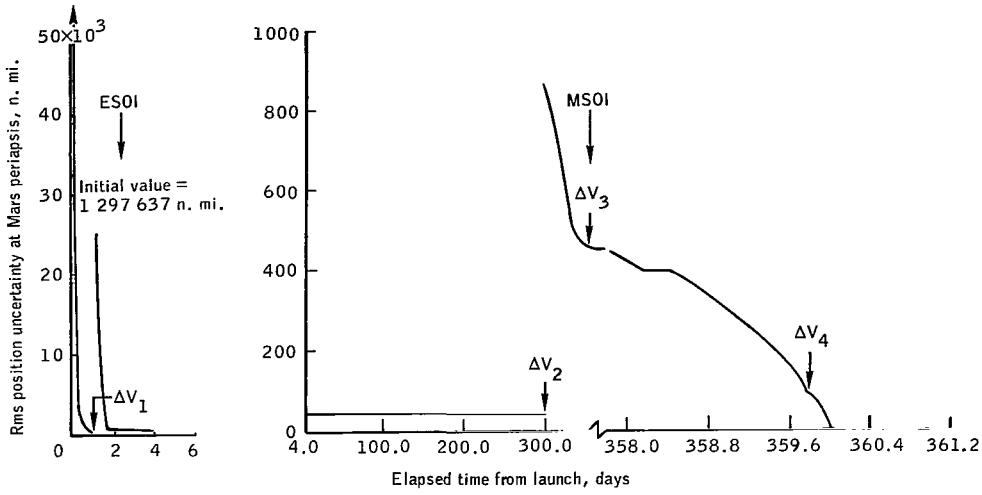

(a) Earth to Mars trajectory.

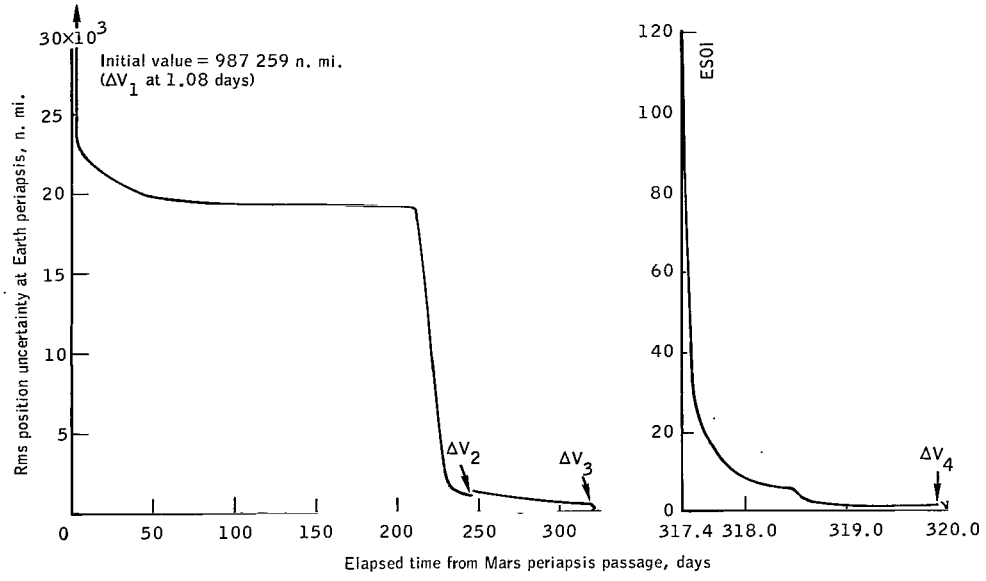

(b) Mars to Earth trajectory.

Figure 15. - Root-mean-square position uncertainty at target-planet periapsis for 1977 Mars stopover mission.

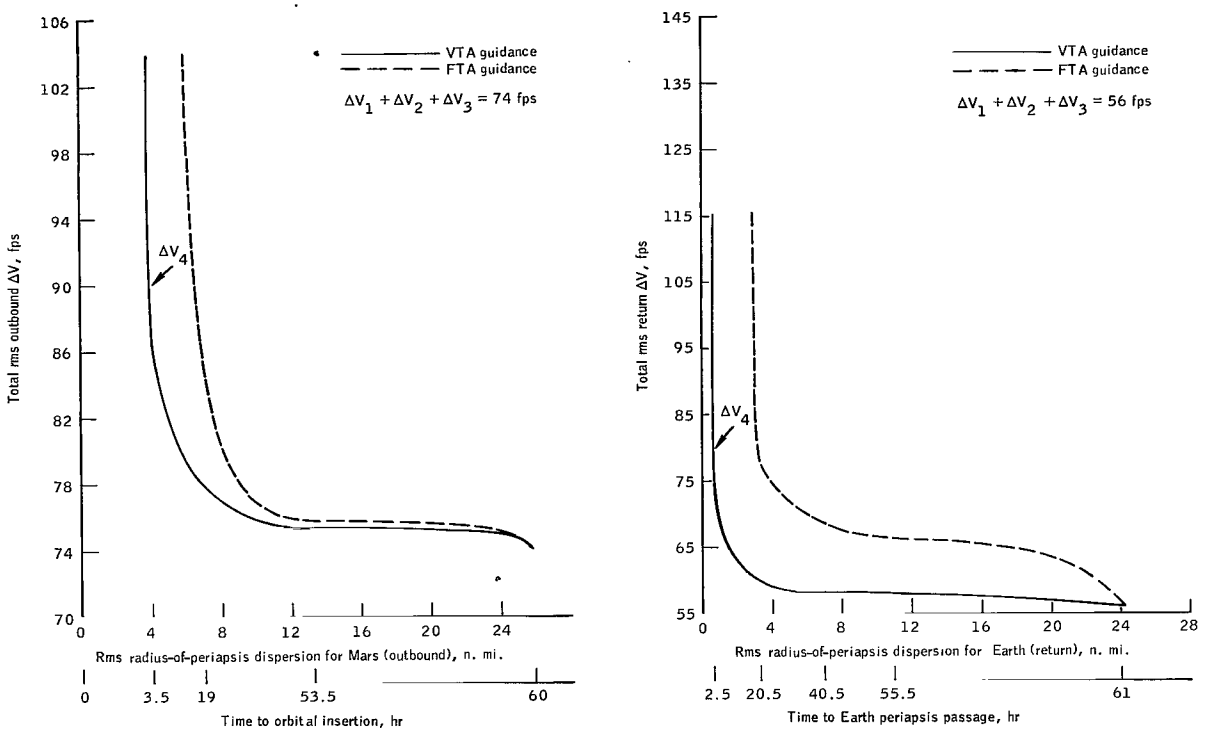

(a) Mars approach phase (outbound). (b) Earth approach phase (return).

Figure 16. - Spacecraft guidance accuracy for 1977 Mars stopover mission.

guidance data curve, it is evident that a delivery accuracy of approximately 4 n. mi. can be obtained by a fourth guidance maneuver execution at 3. 5 hours prior to Mars orbital insertion for an additional velocity change of only 20 fps, or a total outbound midcourse ΔV requirement of 90 fps.

Similarly, from figure 16(b) for the return phase, a delivery accuracy of less than 1 n. mi. can be obtained by making a fourth velocity correction at 2. 5 hours before vacuum perigee for a total return ΔV requirement of approximately 80 fps.

It should be noticed that in comparing the outbound and return phases of the three missions assumed for the analysis, the terminal delivery accuracies of all three missions are approximately equal, whereas the velocity correction requirements for the midcourse guidance maneuvers are considerably less in the 1977 Mars stopover mission than in the two flyby missions. This difference is the result of the basic characteristics of the 1977 Mars stopover mission, especially in the longer phase durations and low passage velocities. A comparison of the characteristics of the three missions is provided in table II.

Spacecraft navigation and guidance, orbital phase. - As previously mentioned, the 1977 Mars stopover mission includes a 300-day stay time in orbit about Mars. The characteristics of this orbit are presented in table III.

Since a navigation and guidance systems analysis for the Mars orbital phase warrants a complete study, only a brief sketch of orbital navigation data is presented, and guidance data are not discussed.

There are several types of orbital navigation techniques that are applicable to this study (ref. 6); however, for the data presented, only one type of navigation was considered for the spacecraft in orbit about Mars. The navigation maneuver simulated was the star-Mars horizon included-angle measurement with a sextant. The measurements were processed throughout the 300-day stay time at 1-hour intervals. This particular maneuver should be applicable to the specific mission studied, since the apoapsis of the orbit is approximately 10 000 n. mi. from Mars and the orbital period is of the order of 0.5 day.

The navigation data obtained for the 300-day orbital phase of the 1977 Mars stopover mission are presented in figure 17. In this figure, the rms position uncertainty is plotted as a function of time in orbit. From figure 17, it is found that the star-horizon navigation measurement controls the rms 1σ position uncertainty to a range between approximately 0.6 and 3.0 n. mi. The interesting feature of figure 17 is the oscillatory behavior of the uncertainty curve. At this time, no specific reason has been given for this effect, although it is believed to result from geometrical effects with respect to both the planetary orbit and the spacecraft orbit. The oscillation directly resulting from each orbit is not shown in the figure because of the scale limitations.

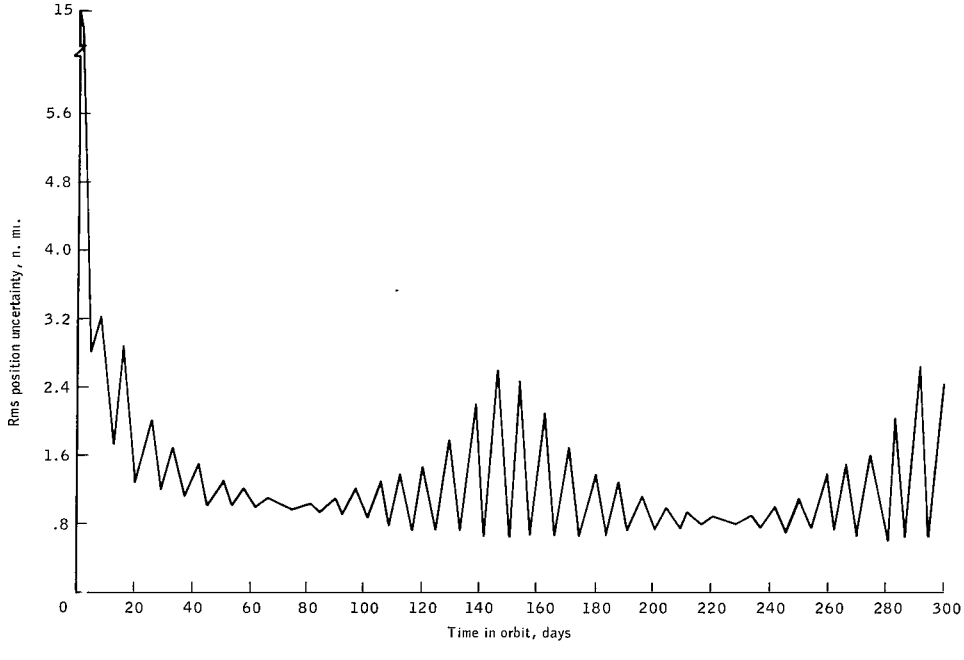

Figure 17. - Orbital navigation accuracy for 1977 Mars stopover mission.

Unmanned-probe navigation and guidance. - Pertinent probe entry parameters for the 1977 Mars stopover mission are plotted in figure 18 as functions of separation velocity. In figure 18(a), the entry data are presented for an entry altitude of 315 000 feet; in figure 18(b), the entry altitude assumed is 405 000 feet. The nominal probe trajectory selected for this mission has an assumed entry altitude of 315 000 feet, an entry speed of 18 350 fps, and an entry flight-path angle of -5°. The resulting probe deployment ΔV is 45 fps.

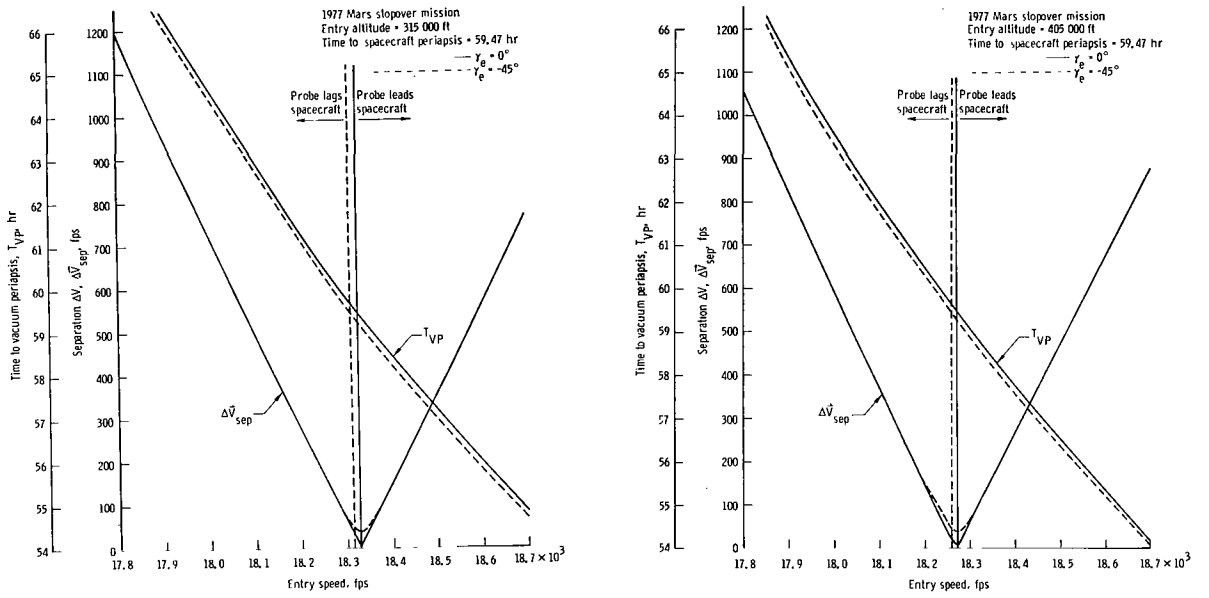

(a) Entry altitude = 315 000 ft.

(b) Entry altitude = 405 000 ft.

Figure 18. - Unmanned-probe entry parameters as a function of separation velocity (1977 Mars stopover mission).

The unmanned-probe navigation results are presented in figure 19 for both the expected and twice the expected onboard-radar errors. The behavior of the data is as expected, and the two curves converge to the same value approximately 58 hours from separation (116 measurements).

The guidance results for the two sets of radar errors are illustrated in figure 20. The increased radar tracking errors have the effect of doubling the ΔV to achieve a specified target dispersion. For example, if a corridor of 30 n. mi. is desired (vacuum radius-of-periapsis dispersion = 5 n. mi.), the ΔV required for expected radar errors is 25 fps; whereas, for twice the expected radar errors, the ΔV requirement increases to almost 50 fps.

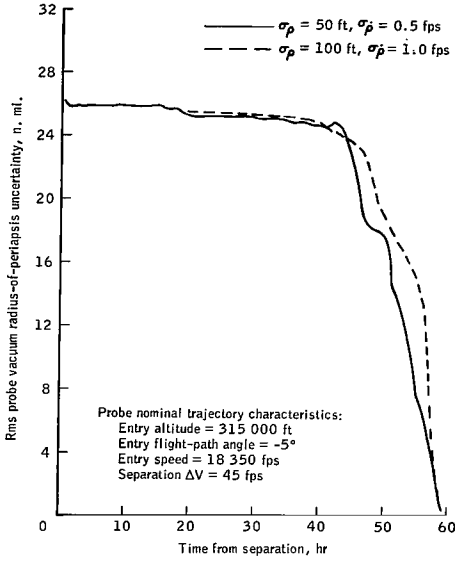

Figure 19. - Unmanned-probe navigation data for 1977 Mars stopover mission.

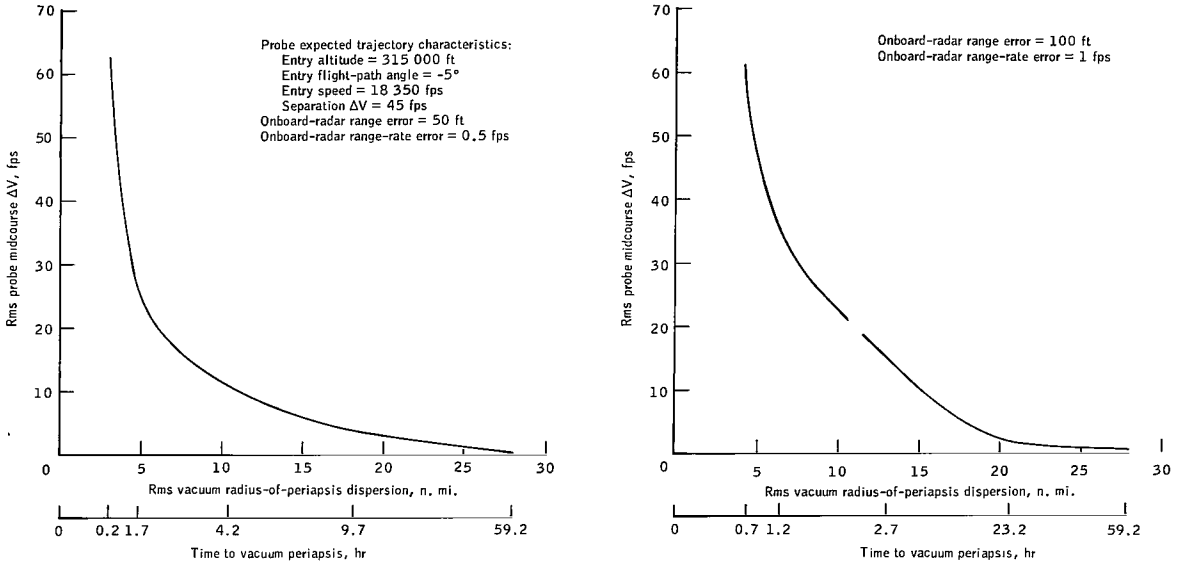

(a) Expected onboard-radar errors.

(b) Twice the expected onboard-radar errors.

Figure 20. - Unmanned-probe guidance data for 1977 Mars stopover mission.

CONCLUDING REMARKS

A navigation and guidance systems analysis for three typical manned interplanetary missions is presented. Performance results are given for three missions: a 1972 Venus flyby mission, a 1975 Mars flyby mission, and a 1977 Mars stopover mission. All phases of each mission were considered, and this consideration included a performance evaluation of both the spacecraft and an unmanned probe in the outbound phase of each mission.

The purpose of the study was not to recommend any specific mission, but to show several interplanetary missions and the similar navigation and guidance systems results obtained.

The midcourse navigation system assumed for the study included Earth-based radar and onboard tracking capabilities for updating state-vector estimates of the spacecraft and probe using a Kalman filter. The guidance system utilized fixed- and variable-time-of-arrival guidance logic for computation of the velocity corrections and appropriate target dispersions.

The results of the performance evaluation in each of the three missions are presented for both the spacecraft and the probe. Excluding the propellant requirements maneuvering in the Mars parking-orbit phase, the results for each mission indicate that a total midcourse ΔV of the order of 200 fps can produce spacecraft delivery accuracies of approximately 4 n. mi. at Mars or Venus and 1 n. mi. at Earth for the outbound and return mission phases, respectively. Similarly, a probe delivery accuracy of somewhat less than 5 n. mi. is achievable with one midcourse correction of approximately 80 fps.

Manned Spacecraft Center
National Aeronautics and Space Administration
Houston, Texas, April 25, 1968
981-30-10-00-72

TABLE I. - EXPECTED 1σ ROOT-MEAN-SQUARE ERROR VALUES

Navigation system:	
Onboard-sextant accuracy, sec of arc	10
Onboard-radar accuracy	
Range, ft	50
Range-rate, fps	0.5
Ratio of planet radius uncertainty to planet radius	
Mars, Venus	0.005
Earth	0.001
Planet position uncertainty, n. mi.	100
Earth-based-radar accuracy	
Range, ft	$\geq 20, \leq 200$
Range-rate, fps	$\geq 0.5, \leq 1.5$
Guidance system:	
Proportional, percent	1
Pointing, deg	1
Cut-off, fps	0.5

TABLE II. - REFERENCE TRAJECTORY CHARACTERISTICS

Trajectory designation	Mission		
	1972 Venus flyby	1975 Mars flyby	1977 Mars stopover
Julian date of launch from Earth	2 441 410.0	2 442 675.0	2 443 400.0
Earth injection velocity magnitude, fps	12 131	15 150	12 652
Outbound trip time, days	111.03	133.29	360
Target-planet stopover time, days	0	0	300
Return trip time, days	251.64	538.64	320
Time in target-planet SOI, hr	60.73	37.74	[a]199.4
Periapsis altitude at target planet, n. mi.	206	106	200
General location of periapsis at target planet (with respect to target-planet equator)	--	Northern hemisphere	Southern hemisphere
Entry velocity at Earth, fps	44 840	47 900	38 463

[a]Plus 300 days in Mars orbit.

TABLE III. - CHARACTERISTICS OF PARKING ORBIT

FOR 1977 MARS STOPOVER MISSION

Orbital stay time, days	300
Periapsis altitude, n. mi.	200
Apoapsis altitude, n. mi.	9 621.67
Inclination, deg	41.82
Eccentricity	0.697
Period, hr	11.78
Periapsis velocity, hyperbolic approach, fps	17 800
Periapsis velocity, orbital, fps	14 403
Apoapsis velocity, orbital, fps	2 568
Periapsis velocity, hyperbolic departure, fps	18 395

TABLE IV. - MIDCOURSE ΔV AND TARGET-PLANET DISPERSION SUMMARY

Mission	Phase	Root-mean-square midcourse ΔV, fps					Root-mean-square target-planet dispersions, n. mi.		
		ΔV_1	ΔV_2	ΔV_3	ΔV_4	Total	Radius	Range	Track
1977 Mars stopover	Outbound	45.95	16.13	12.04	[a]14.42	88.54	3.89	448.00	1.45
	Return	22.35	12.51	21.43	[a]21.03	77.32	.68	1030.04	.23
1975 Mars flyby	Outbound	43.14	10.26	6.10	[a]22.55	82.05	3.88	81.73	3.83
	Return	32.36	24.45	78.64	[a]36.30	171.75	1.09	871.04	.71
1972 Venus flyby	Outbound	50.44	25.95	[a]19.77	--	96.16	4.09	121.16	1.47
	Return	35.36	20.54	29.81	[a]30.97	116.68	.99	389.68	.59

[a]These corrections were obtained using VTA guidance logic.

TABLE V. - PROBE ΔV AND DISPERSION SUMMARY

Mission	Onboard-radar error		Separation ΔV, fps	Midcourse ΔV, fps	Total ΔV, fps	Vacuum radius-of-periapsis dispersion, n. mi.
	Range, ft	Range-rate, fps				
1977 Mars stopover	50	0.5	45.57	62.65	108.22	3.06
	100	1.0	45.57	61.13	106.70	4.34
1975 Mars flyby	50	0.5	14.32	81.11	95.43	4.13
	100	1.0	14.32	80.90	95.22	6.87
1972 Venus flyby	50	0.5	49.39	51.87	101.26	3.51
	100	1.0	49.39	51.58	100.97	3.60

APPENDIX

SPACECRAFT/PROBE NAVIGATION-SYSTEM EQUATIONS

The spacecraft/probe tracking geometry is illustrated in the following sketch. For this study, it was assumed that the spacecraft onboard radar would measure the relative range and range-rate to the probe and simultaneously use an onboard optical sensor (i.e., sextant) to measure the included angle between the target-planet horizon and a star. This procedure is feasible since the onboard radar can track the probe continuously; and when the spacecraft horizon-star angular measurement is fed into the onboard computer, a command can automatically be set up in the navigation program to call for simultaneous data processing of the radar range and range-rate information.

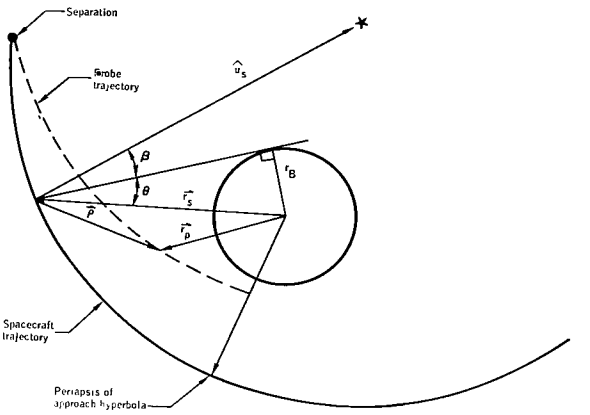

The data can be processed in the onboard computer using an augmented Kalman filter (refs. 7 and 8). The details of this type of filter are collectively discussed in references 1, 2, 3, 7, and 8; and the derivation of the filter algorithm is presented in reference 4. Therefore, further description of the standard Kalman filter is unnecessary. The structure of the augmented filter equations used is identical to the standard Kalman-filter equations but with increased state-vector dimensions. For the problem considered here, the state vector is 12-dimensional and includes the spacecraft position and velocity, as well as the unmanned-probe position and velocity. The equation which relates deviations in this state vector at time t to deviations at time t_0 is

$$\begin{bmatrix} \delta\vec{r}_s(t) \\ \delta\vec{V}_s(t) \\ \delta\vec{r}_p(t) \\ \delta\vec{V}_p(t) \end{bmatrix} = \begin{bmatrix} \Phi(t,t_0) & 0 \\ 0 & \Gamma(t,t_0) \end{bmatrix} \begin{bmatrix} \delta\vec{r}_s(t_0) \\ \delta\vec{V}_s(t_0) \\ \delta\vec{r}_p(t_0) \\ \delta\vec{V}_p(t_0) \end{bmatrix} \tag{3}$$

where $\Phi(t, t_0)$ and $\Gamma(t, t_0)$ are the spacecraft and probe 6×6 state transition matrices, respectively. If

$$\vec{\xi}(t) = \begin{bmatrix} \delta\vec{r}_s(t) \\ \delta\vec{V}_s(t) \\ \delta\vec{r}_p(t) \\ \delta\vec{V}_p(t) \end{bmatrix} \tag{4}$$

and

$$\Theta(t, t_0) = \begin{bmatrix} \Phi(t, t_0) & 0 \\ 0 & \Gamma(t, t_0) \end{bmatrix} \tag{5}$$

then equation (3) becomes

$$\vec{\xi}(t) = \Theta(t, t_0)\vec{\xi}(t_0) \tag{6}$$

The initial 12×12 covariance matrix for the augmented system, that is, at spacecraft/probe separation, is

$$P(t_{sep}) = \begin{bmatrix} E_s(t_{sep}) & 0 \\ 0 & E_p(t_{sep}) \end{bmatrix} \tag{7}$$

where $E_s(t_{sep})$ is the spacecraft uncertainty covariance matrix and $E_p(t_{sep}) = E_s(t_{sep}) + \Delta E(t_{sep})$. The term $\Delta E(t_{sep})$ is the degradation to the probe uncertainty matrix as a result of an imperfect separation maneuver. The equation for propagating the augmented covariance matrix between measurements is

$$P(t) = \Theta(t, t_0)P(t_0)\Theta^T(t, t_0) \tag{8}$$

The equation which relates deviations in the observables to state-vector deviations is

$$\begin{bmatrix} \delta\beta(t) \\ \delta\rho(t) \\ \delta\dot{\rho}(t) \end{bmatrix} = H(t)\vec{\xi}(t) \tag{9}$$

where the 3×12 matrix $H(t)$ is written in partitioned form as

$$H(t) = \begin{bmatrix} A(t) & 0 \\ -B(t) & B(t) \end{bmatrix} \tag{10}$$

The 1×6 vector $A(t)$ is

$$A(t) = \begin{bmatrix} \dfrac{\partial\beta}{\partial\vec{r}_s} & \dfrac{\partial\beta}{\partial\vec{V}_s} \end{bmatrix} \tag{11}$$

and the 2×6 matrix $B(t)$ is

$$B(t) = \begin{bmatrix} \dfrac{\partial\rho}{\partial\vec{\rho}} & \dfrac{\partial\rho}{\partial\vec{V}_\rho} \\ \dfrac{\partial\dot{\rho}}{\partial\vec{\rho}} & \dfrac{\partial\dot{\rho}}{\partial\vec{V}_\rho} \end{bmatrix} \tag{12}$$

The partial derivatives required in equations (11) and (12) can be calculated from the following relationships. (Also, refer to the sketch presented previously.)

$$\left.\begin{aligned} \frac{\partial\beta}{\partial\vec{r}_s} &= \frac{r_B}{r_s^3 \cos\theta}\vec{r}_s + \frac{\vec{r}_s \times \left(\vec{r}_s \times \hat{u}_s\right)}{r_s^2 \left|\vec{r}_s \times \hat{u}_s\right|} \\ \frac{\partial\beta}{\partial\vec{V}_s} &= 0 \end{aligned}\right\} \tag{13}$$

$$\left.\begin{aligned}
\frac{\partial \rho}{\partial \vec{\rho}} &= \frac{\vec{\rho}^{T}}{\rho} \\
\frac{\partial \rho}{\partial \vec{V}_{\rho}} &= 0 \\
\frac{\partial \dot{\rho}}{\partial \vec{\rho}} &= \frac{\vec{V}_{\rho}^{T}}{\rho}\left(I - \frac{\vec{\rho}\vec{\rho}^{T}}{\rho^{2}}\right) \\
\frac{\partial \dot{\rho}}{\partial \vec{V}_{\rho}} &= \frac{\vec{\rho}^{T}}{\rho}
\end{aligned}\right\} \qquad (14)$$

The equations required to update the augmented uncertainty matrix $P(t)$ at the time of a measurement can now be written

$$\left.\begin{aligned}
P^{+}(t) &= [I - K(t)H(t)]\,P^{-}(t) \\
K(t) &= P^{-}(t)H^{T}(t)M^{-1}(t) \\
M(t) &= H(t)P^{-}(t)H^{T}(t) + R(t)
\end{aligned}\right\} \qquad (15)$$

where the 3×3 covariance matrix of measurement errors $R(t)$ is

$$R(t) = \begin{bmatrix} \sigma_{\beta}^{2} & 0 & 0 \\ 0 & \sigma_{\rho}^{2} & 0 \\ 0 & 0 & \sigma_{\dot{\rho}}^{2} \end{bmatrix} \qquad (16)$$

and the superscripts - and + refer to a quantity before and after the measurement, respectively.

REFERENCES

1. Cicolani, Luigi S.: Interplanetary Midcourse Guidance Using Radar Tracking and On-Board Observation Data. NASA TN D-3623, 1966.

2. Murtagh, Thomas B.; Lowes, Flora B.; and Bond, Victor R.: Navigation and Guidance Analysis of a Mars Probe Launched From a Manned Flyby Spacecraft. NASA TN D-4512, 1968.

3. White, John S.; Callas, George P.; and Cicolani, Luigi S.: Application of Statistical Filter Theory to the Interplanetary Navigation and Guidance Problem. NASA TN D-2697, 1965.

4. Battin, Richard H.: Astronautical Guidance. McGraw-Hill Book Co., Inc., 1964.

5. Rohde, Paul J.: The Schedule of Measurements for Analysis of an Onboard Navigation System. NASA-CR-61107, 1965.

6. Baker, D. S.; Sears, N. E.; and White, R. L.: Lunar Orbit Navigation Performance With Various Random and Systematic Errors. MIT Instrumentation Laboratory Report E-1983, 1966.

7. Suddath, J. H.; Kidd, Robert H. III; and Reinhold, Arnold G.: A Linearized Error Analysis of Onboard Primary Navigation Systems for the Apollo Lunar Module. NASA TN D-4027, 1967.

8. Murtagh, Thomas B.: Analysis of Sextant Navigation Measurements During Lunar Module Rendezvous. NASA TN D-3873, 1967.

NATIONAL AERONAUTICS AND SPACE ADMINISTRATION
WASHINGTON, D.C. 20546

OFFICIAL BUSINESS

FIRST CLASS MAIL

POSTAGE AND FEES PAID
NATIONAL AERONAUTICS AND
SPACE ADMINISTRATION

POSTMASTER: If Undeliverable (Section 158 Postal Manual) Do Not Return

"The aeronautical and space activities of the United States shall be conducted so as to contribute . . . to the expansion of human knowledge of phenomena in the atmosphere and space. The Administration shall provide for the widest practicable and appropriate dissemination of information concerning its activities and the results thereof."

—NATIONAL AERONAUTICS AND SPACE ACT OF 1958

NASA SCIENTIFIC AND TECHNICAL PUBLICATIONS

TECHNICAL REPORTS: Scientific and technical information considered important, complete, and a lasting contribution to existing knowledge.

TECHNICAL NOTES: Information less broad in scope but nevertheless of importance as a contribution to existing knowledge.

TECHNICAL MEMORANDUMS: Information receiving limited distribution because of preliminary data, security classification, or other reasons.

CONTRACTOR REPORTS: Scientific and technical information generated under a NASA contract or grant and considered an important contribution to existing knowledge.

TECHNICAL TRANSLATIONS: Information published in a foreign language considered to merit NASA distribution in English.

SPECIAL PUBLICATIONS: Information derived from or of value to NASA activities. Publications include conference proceedings, monographs, data compilations, handbooks, sourcebooks, and special bibliographies.

TECHNOLOGY UTILIZATION PUBLICATIONS: Information on technology used by NASA that may be of particular interest in commercial and other non-aerospace applications. Publications include Tech Briefs, Technology Utilization Reports and Notes, and Technology Surveys.

Details on the availability of these publications may be obtained from:

SCIENTIFIC AND TECHNICAL INFORMATION DIVISION

NATIONAL AERONAUTICS AND SPACE ADMINISTRATION

Washington, D.C. 20546